Research article

A ternary mixture model with dynamic boundary conditions

Shuang Liu[1], Yue Wu[2] and Xueping Zhao[2,∗]

[1] Department of Mathematics, University of North Texas, 1155 Union Circle, Denton, Texas 76203-5017, USA

[2] Department of Mathematical Sciences, University of Nottingham Ningbo China, Taikang East Road 199, Ningbo 315100, China

* **Correspondence:** Email: Xueping.Zhao@nottingham.edu.cn.

Abstract: The influence of short-range interactions between a multi-phase, multi-component mixture and a solid wall in confined geometries is crucial in life sciences and engineering. In this work, we extend the Cahn-Hilliard model with dynamic boundary conditions from a binary to a ternary mixture, employing the Onsager principle, which accounts for the cross-coupling between forces and fluxes in both the bulk and surface. Moreover, we have developed a linear, second-order and unconditionally energy-stable numerical scheme for solving the governing equations by utilizing the invariant energy quadratization method. This efficient solver allows us to explore the impacts of wall-mixture interactions and dynamic boundary conditions on phenomena like spontaneous phase separation, coarsening processes and the wettability of droplets on surfaces. We observe that wall-mixture interactions influence not only surface phenomena, such as droplet contact angles, but also patterns deep within the bulk. Additionally, the relaxation rates control the droplet spreading on surfaces. Furthermore, the cross-coupling relaxation rates in the bulk significantly affect coarsening patterns. Our work establishes a comprehensive framework for studying multi-component mixtures in confined geometries.

Keywords: phase-field model; ternary mixture; dynamic boundary condition; energy stability; wetting

1. Introduction

The physics of multi-component mixtures, including spontaneous phase separation, nucleation and growth and coarsening have been well-studied both theoretically and experimentally. The question of how the multi-component, multi-phase system interacts with solid walls in confined geometries has gained much attention due to its wide applications in life science and engineering, e.g., membrane-less organelle formation and wetting on the membrane-bound organelles in living cells [1–3]; micro-fluid

close to a solid interface in microfluidic devices [4]; thin films of polymer blends in slab geometry [5–7] and so on.

Numerous methods have been developed to study interface problems and their interaction with solid walls. For instance, the lattice Boltzmann model has garnered considerable attention as a tool to facilitate the simulation of multi-phase and multi-component systems with complex boundary conditions, as demonstrated by several studies [8–12]. Additionally, the exploration of wetting properties in ternary mixture models has been a significant focus [13–15]. For example, Liang et al. [16] formulated a wetting boundary condition for ternary fluids interacting with a solid substrate, applying this to the lattice Boltzmann model. The volume-of-fluid (VOF) technique is particularly effective in scenarios involving solid obstacles, as it integrates the contact angle by applying appropriate boundary conditions to the fluid-function's gradient at solid interfaces. Therefore, VOF has been extensively used in fluid dynamics analyses within complex porous structures [17–21]. However, among all of these methods, the phase-field method stands out as the most effective tool for modeling and simulating multi-phase systems. Its inherent flexibility in handling complex topological changes in the phases, coupled with its ability to seamlessly integrate with various boundary conditions, makes it a superior choice to address the complexities of interface problems in multi-component systems.

The Cahn-Hilliard equation is a fundamental phase-field model. Since it was first proposed in the field of materials science to describe the pattern formation evolution of microstructures during the phase separation process in binary alloys [22, 23], the Cahn-Hilliard equation and its variants have been successfully applied to model a wide variety of segregation-like phenomena in science; see, for instance, [24–31] and the references therein. In this study, we denote the domain as Ω and the boundary of the domain Γ. We introduce ϕ, which represents the volume fraction of a specific component within the mixture. $\phi \in (0, 1)$ is dimensionless and quantifies the proportion of the total volume occupied by a given component, providing insight into the concentration and distribution of that component within the system. The total free energy of the system is given as

$$F = \int_{\Omega} \left[f_b(\phi) + \frac{\kappa}{2} |\nabla \phi|^2 \right] d\boldsymbol{x}, \tag{1.1}$$

where $f_b(\phi)$ is the bulk free-energy density function and the term $\frac{\kappa}{2} |\nabla \phi|^2$ represents the interfacial energy between phases. The Cahn-Hilliard equation has the following format:

$$\partial_t \phi = \nabla M \cdot \nabla \mu, \tag{1.2}$$

where mobility M can be either a constant or concentration-dependent function and μ is the chemical potential of the component ϕ. The boundary conditions include the following two categories:

1) periodic boundary conditions,

2) physical boundary conditions, e.g., homogeneous Neumann boundary conditions.

However, in some systems, e.g., phase separation in confined geometries, the condensate will interplay with boundaries; thus more generic boundary conditions, which describe the interaction between wall and condensates, are introduced. In this work, we will focus on the study of generic boundary conditions.

The influence of boundaries (solid walls) on the phase separation process of binary mixtures has attracted a lot of attention from scientists. For instance, Fischer et al. [27] introduced the following

dynamic boundary conditions in 1997:

$$\partial_n \mu|_\Gamma = 0, \tag{1.3a}$$

$$\partial_t \phi|_\Gamma = -\Gamma_s \Big[\kappa\, \partial_n \phi + f_s{}' - \kappa_\Gamma \Delta_\Gamma \phi_\Gamma \Big], \tag{1.3b}$$

where f_s is the surface free-energy density, which represents the short-range interaction between mixture components and the solid wall, Δ_Γ stands for the Laplace–Beltrami operator on the boundary surface Γ, Γ_s defines a surface kinetic coefficient and the term $\kappa\, \partial_n \phi$ is due to the surface contribution that comes from the variation of the bulk free energy f_b. The boundary (1.3a) is simply the condition that no current can flow through the surface, while the boundary (1.3b) can be derived by requiring the system to tend to minimize its surface free energy as follows:

$$F_s = \int_\Omega \Big[\frac{\kappa_\Gamma}{2} |\nabla_\Gamma \phi_\Gamma|^2 + f_s \Big]. \tag{1.4}$$

Boundary conditions of similar form as (1.3) have also been derived from a semi-infinite Ising model with Kawasaki spin exchange dynamics [32, 33]. In 2011, Goldstein et al. derived a Cahn-Hilliard model in a domain with non-permeable walls [29]. In this model, they assumed that the total mass in the bulk and on the boundary, i.e.,

$$\int_\Omega \phi(\boldsymbol{x})d\boldsymbol{x} + \int_\Gamma \phi(\boldsymbol{x})dS, \tag{1.5}$$

is conserved. Its boundary conditions are as follows:

$$\partial_t \phi|_\Gamma = \nabla_\Gamma M \cdot \nabla_\Gamma \mu_\Gamma - \beta M \partial_n \mu, \tag{1.6a}$$

$$\mu|_\Gamma = \beta \Big[\kappa\, \partial_n \phi + f_s{}' - \kappa_\Gamma \Delta_\Gamma \phi_\Gamma \Big]. \tag{1.6b}$$

In addition, they proved the existence and uniqueness of weak solutions and studied their asymptotic behavior as time goes to infinity.

Liu and Wu [30] introduced a Liu-Wu model in 2019 with non-flux boundary conditions for chemical potential and Cahn–Hilliard-type gradient flow on the boundary, i.e.,

$$\partial_n \mu = 0, \tag{1.7a}$$

$$\partial_t \phi|_\Gamma = \nabla_\Gamma M \cdot \nabla_\Gamma \Big[\kappa\, \partial_n \phi + f_s{}' - \kappa_\Gamma \Delta_\Gamma \phi_\Gamma \Big]. \tag{1.7b}$$

In 2021, Patrik Knopf and collaborators proposed a general model, i.e., the KLLM model [31]:

$$L \partial_n \mu = -\mu|_\Gamma + \beta \Big[\kappa\, \partial_n \phi + f_s{}' - \kappa_\Gamma \Delta_\Gamma \phi_\Gamma \Big], \tag{1.8a}$$

$$\partial_t \phi|_\Gamma = \nabla_\Gamma M \cdot \nabla_\Gamma \Big[\kappa\, \partial_n \phi + f_s{}' - \kappa_\Gamma \Delta_\Gamma \phi_\Gamma \Big] - \beta M \partial_n \mu. \tag{1.8b}$$

Garcke et al. [34] performed nonlinear analysis to evaluate the long-time dynamics of the Cahn–Hilliard equation with kinetic rate dependent dynamic boundary conditions for the KLLM model. We refer the reader to [35] for a review of the model and analysis.

Correspondingly, there are numerical studies for binary mixture models with dynamic boundary conditions. For example, Kenzler et al. [28] proposed an implicit numerical scheme to solve the

Cahn–Hilliard equation with (1.3). The authors discretized the solution in space by applying the finite-difference method to edge points. A method of stability analysis was derived and a variable time-stepping strategy was employed to simulate the system over a long period of time. Furthermore, the numerical scheme is conditionally gradient-stable, which means that the free energy decreases monotonously in time. In 2017, Fukao et al. [36] constructed a structure-preserving finite-difference scheme for the Cahn–Hilliard equation with dynamic boundary conditions in the one-dimensional case for Goldstein model (1.6). Unlike the space discretization in [28], the authors applied the finite-difference method to center points. The existence of the solution and the error estimate were also obtained. In addition, the laws of mass conservation and energy dissipation were satisfied at the discrete level. Meng et al. [37] developed a second-order stabilized semi-implicit scheme for Liu-Wu model (1.7). The corresponding energy stability and convergence analysis of the scheme were derived theoretically.

Besides the binary mixture models, phase-field models for ternary mixture systems have been developed due to their frequent real-world applications, as indicated in the literature [38–40]. Wetting behavior [41, 42] has also been proposed based on the phase-field models. For example, a phase-field model for multi-component Cahn-Hilliard systems in complex domains was developed in [41] by considering contact angle or no mass flow boundary conditions. Building on this, Yang et al. [42] extended the geometric formulation of wetting conditions by using the weighted contact angles defined within the implementation of wetting conditions, following the concept of the diffusive interface [43]. This innovative phase-field model efficiently describes the dynamic behavior of compound droplets in contact with solid objects.

However, we note that dynamic boundary conditions are missing in the aforementioned multi-component phase-field models. Moreover, to the best of our knowledge, a ternary mixture model with the force-flux cross-coupling relations has not been explored yet. In summary, based on the above discussion, we focus on the following aims in this work:

1) Derive a model for a ternary mixture with the force-flux cross-coupling relations in a confined geometry with dynamic boundary conditions based on the Onsager principle and irreversible thermodynamics [44–49].

2) Develop a linear second-order unconditionally energy-stable numerical scheme for the derived model based on the invariant energy quadratization (IEQ) method [50–53].

3) Investigate equilibrium and non-equilibrium properties of the system based on the numerical simulations.

Section 2 details the derivation of a kinetic model. This model, which addresses a ternary mixture within confined geometries and its interaction with adjacent solid walls, is formulated by using principles of irreversible thermodynamics. It features a conservation of total mass and a decrease in total energy over time. The mathematical model undergoes an equivalent reformulation based on the IEQ method in Section 3, where we also introduce a second-order, linear, unconditional energy-stable numerical scheme for the revised model. Section 4 examines how spontaneous phase separation and surface wettability are influenced by various model parameters through the use of numerical studies. The paper concludes in Section 5, where we summarize our findings. For clarity, we list abbreviations and notations in Tables 1 and 2.

Table 1. Abbreviations.

Abbreviations	Explanations
DBC	Dynamic boundary condition
IEQ	Invariant energy quadratization

Table 2. Notations.

Notations	Explanations
χ_{ij}	interaction strength between the components i and j
γ	coupling interaction strength between components on the surface
Γ	boundary of domain
Γ_i	relaxation parameter of dynamic boundary condition, i=1, 2, 12
Γ_s	surface kinetic coefficient
κ_B	Boltzmann constant
$\kappa_i, \kappa_{i\Gamma}$	gradient coefficients associated with interface free energies, i=1, 2, 12
μ_i	chemical potential in the bulk for components i=1, 2
$\mu_{i\Gamma}$	chemical potential on the surface for components i=1, 2
Δ_Γ	Laplace–Beltrami operator on the boundary surface
ν	molecular volume of component 3
ν_i	molecular volume of component i, i=1, 2
Ω	domain
ω_i	internal free energy coefficient for component i in the bulk
ϕ_i	volume fraction of three components, i=1, 2, 3
$\phi_{i\Gamma}$	volume fraction of a component, i=1, 2
D_i	diffusion coefficients, i=1, 2, 12
f_b	bulk free-energy density function
f_s	surface free-energy density function
g_i	molecule-molecule interaction strength of each component near the wall
h_i	interaction strength proportional to the component volume fraction, i=1, 2
J_i	mass flux, i=1, 2
M_i	mobility function, i=1, 2, 12
T	temperature of the isotropic system

2. Mathematical model derivation

In this section, we will extend the binary mixture model with dynamic boundary conditions to a ternary mixture model, based on the Onsager principles [44–48]. We denote the volume fractions of three components as ϕ_1, ϕ_2 and ϕ_3, where $\phi_3 = 1 - \phi_1 - \phi_2$ based on the incompressibility assumption.

The total free energy of the system involves two contributions: one is the free energy in the bulk Ω, and another on the surface Γ, i.e.,

$$E = E_{\text{bulk}} + E_{\text{surf}}, \tag{2.1}$$

where the bulk free energy E_{bulk} and surface free energy E_{surface} are as follows:

$$E_{\text{bulk}} = \int_{\Omega} \left[f_b(\phi_1, \phi_2) + \frac{\kappa_1}{2} |\nabla \phi_1|^2 + \frac{\kappa_2}{2} |\nabla \phi_2|^2 + \kappa_{12} \nabla \phi_1 \cdot \nabla \phi_2 \right], \tag{2.2}$$

$$E_{\text{surf}} = \int_{\Gamma} \left[f_s(\phi_{1\Gamma}, \phi_{2\Gamma}) + \frac{\kappa_{1\Gamma}}{2} |\nabla_\Gamma \phi_{1\Gamma}|^2 + \frac{\kappa_{2\Gamma}}{2} |\nabla_\Gamma \phi_{2\Gamma}|^2 + \kappa_{12\Gamma} \nabla_\Gamma \phi_{1\Gamma} \cdot \nabla_\Gamma \phi_{2\Gamma} \right]. \tag{2.3}$$

κ_i, $\kappa_{i\Gamma}$, $i = 1, 2, 12$ denote the gradient coefficients associated with interface free energies. For simplicity, we set $\kappa_{12} = 0$ and $\kappa_{12\Gamma} = 0$ in the following work. ∇_Γ denotes the gradient operator on the surface. The bulk free-energy density function $f_b(\phi_1, \phi_2)$ and surface free-energy density function $f_s(\phi_{1\Gamma}, \phi_{2\Gamma})$ are defined as the Flory-Huggins free energy and a second-order polynomial based on application in the polymer field [54]:

$$\begin{aligned} f_b(\phi_1, \phi_2) = \frac{k_B T}{\nu} \Big[&\frac{\phi_1}{n_1} \ln \phi_1 + \frac{\phi_2}{n_2} \ln \phi_2 + (1 - \phi_1 - \phi_2) \ln(1 - \phi_1 - \phi_2) + \chi_{12} \phi_1 \phi_2 \\ &+ \chi_{13} \phi_1 (1 - \phi_1 - \phi_2) + \chi_{23} \phi_2 (1 - \phi_1 - \phi_2) + \omega_1 \phi_1 + \omega_2 \phi_2 \Big], \end{aligned} \tag{2.4}$$

$$f_s(\phi_{1\Gamma}, \phi_{2\Gamma}) = \frac{k_B T}{\nu_s} \Big[h_1 \phi_{1\Gamma} + g_1 \phi_{1\Gamma}^2 + h_2 \phi_{2\Gamma} + g_2 \phi_{2\Gamma}^2 + \gamma \phi_{1\Gamma} \phi_{2\Gamma} \Big], \tag{2.5}$$

where $\nu_i = n_i \nu$ represents the molecular volume of component i, $i = 1, 2$, and ν represents the molecular volume of component 3. For simplicity, we assume the molecular volumes of each component are equivalent, i.e., $\nu_1 = \nu_2 = \nu$ and $n_1 = n_2 = 1$. k_B is the Boltzmann constant and T is the temperature of the isotropic system. The term $\chi_{ij} \phi_i \phi_j$ refers to the interaction strength between the component i and the component j. $\omega_i \phi_i$ denotes the internal free energy for component i in the bulk Ω. On the surface, $h_i \phi_i$, $i = 1, 2$ is the linear order term, which denotes the interaction strength as is proportional to the component volume fraction. The quadratic $g_i \phi_i^2$ depicts the molecule-molecule interactions of each components near the wall, while $\gamma \phi_1 \phi_2$ describes the coupling interaction between components on the surface.

We assume that there is no chemical reaction in the system, that is, each component of the mixture conserves the total mass. We write the conservation laws as follows:

$$\partial_t \phi_1 + \nabla \cdot \boldsymbol{J_1} = 0, \tag{2.6}$$

$$\partial_t \phi_2 + \nabla \cdot \boldsymbol{J_2} = 0. \tag{2.7}$$

2.1. Irreversible thermodynamics

We consider a closed system in this work. According to irreversible thermodynamics, the entropy product rate is inversely proportional to the energy change rate.

$$-T \partial_t S = \frac{dE}{dt} = \frac{\partial E}{\partial \phi_1} \frac{\partial \phi_1}{\partial t} + \frac{\partial E}{\partial \phi_2} \frac{\partial \phi_2}{\partial t} + \frac{\partial E}{\partial \phi_{1\Gamma}} \frac{\partial \phi_{1\Gamma}}{\partial t} + \frac{\partial E}{\partial \phi_{2\Gamma}} \frac{\partial \phi_{2\Gamma}}{\partial t}$$

$$+ \frac{\partial E}{\partial \nabla \phi_1}\frac{\partial \nabla \phi_1}{\partial t} + \frac{\partial E}{\partial \nabla \phi_2}\frac{\partial \nabla \phi_2}{\partial t} + \frac{\partial E}{\partial \nabla_\Gamma \phi_{1\Gamma}}\frac{\partial \nabla_\Gamma \phi_{1\Gamma}}{\partial t} + \frac{\partial E}{\partial \nabla_\Gamma \phi_{2\Gamma}}\frac{\partial \nabla_\Gamma \phi_{2\Gamma}}{\partial t} \tag{2.8}$$

$$= \int_\Gamma dS \Big[\boldsymbol{n} \cdot \kappa_1 \nabla \phi_1 + (\frac{\partial f_s}{\partial \phi_{1\Gamma}} - \kappa_{1\Gamma}\Delta_\Gamma \phi_1) \Big]\frac{\partial \phi_{1\Gamma}}{\partial t}$$

$$+ \int_\Gamma dS \Big[\boldsymbol{n} \cdot \kappa_2 \nabla \phi_2 + (\frac{\partial f_s}{\partial \phi_{2\Gamma}} - \kappa_{2\Gamma}\Delta_\Gamma \phi_2) \Big]\frac{\partial \phi_{2\Gamma}}{\partial t}$$

$$- \int_\Gamma dS \Big[\frac{\mu_1}{\nu_1}\boldsymbol{n} \cdot \boldsymbol{J_1} + \frac{\mu_2}{\nu_2}\boldsymbol{n} \cdot \boldsymbol{J_2} \Big] + \int_\Omega dx \Big[\nabla\frac{\mu_1}{\nu_1} \cdot \boldsymbol{J_1} + \nabla\frac{\mu_2}{\nu_2} \cdot \boldsymbol{J_2} \Big], \tag{2.9}$$

where the chemical potentials in the bulk for components 1 and 2 are respectively defined as

$$\mu_1 = \nu_1 \frac{\delta E}{\delta \phi_1} = \nu_1 \Big[\frac{\partial f_b}{\partial \phi_1} - \kappa_1 \Delta \phi_1 \Big], \tag{2.10}$$

$$\mu_2 = \nu_2 \frac{\delta E}{\delta \phi_2} = \nu_2 \Big[\frac{\partial f_b}{\partial \phi_2} - \kappa_2 \Delta \phi_2 \Big]. \tag{2.11}$$

We obtain the conjugate fluxes and forces as follows:

$$\boldsymbol{J_1} \longleftrightarrow -\nabla\mu_1, \qquad\qquad x \in \Omega, \tag{2.12a}$$

$$\boldsymbol{J_2} \longleftrightarrow -\nabla\mu_2, \qquad\qquad x \in \Omega, \tag{2.12b}$$

$$\partial_t \phi_{1\Gamma} \longleftrightarrow -\Big(\boldsymbol{n} \cdot \kappa_1 \nabla \phi_1 + \frac{\partial f_s}{\partial \phi_{1\Gamma}} - \kappa_{1\Gamma}\Delta_\Gamma \phi_1 \Big), \qquad\qquad x \in \Gamma, \tag{2.12c}$$

$$\partial_t \phi_{2\Gamma} \longleftrightarrow -\Big(\boldsymbol{n} \cdot \kappa_2 \nabla \phi_2 + \frac{\partial f_s}{\partial \phi_{2\Gamma}} - \kappa_{2\Gamma}\Delta_\Gamma \phi_2 \Big), \qquad\qquad x \in \Gamma. \tag{2.12d}$$

Based on the Onsager principle, we define a symmetric positive definite mobility function between conjugate fluxes and forces in both the bulk Ω and the surface Γ, i.e.,

$$\boldsymbol{J_1} = -M_1(\phi_1, \phi_2)\nabla\mu_1 - M_{12}(\phi_1, \phi_2)\nabla\mu_2, \tag{2.13a}$$

$$\boldsymbol{J_2} = -M_{12}(\phi_1, \phi_2)\nabla\mu_1 - M_2(\phi_1, \phi_2)\nabla\mu_2, \tag{2.13b}$$

$$\partial_t \phi_{1\Gamma} = -\Gamma_1 \Big[\boldsymbol{n} \cdot \kappa_1 \nabla \phi_1 - \kappa_{1\Gamma}\Delta_\Gamma \phi_{1\Gamma} + \frac{\partial f_s}{\partial \phi_{1\Gamma}} \Big] - \Gamma_{12} \Big[\boldsymbol{n} \cdot \kappa_2 \nabla \phi_2 - \kappa_{2\Gamma}\Delta_\Gamma \phi_{2\Gamma} + \frac{\partial f_s}{\partial \phi_{2\Gamma}} \Big], \tag{2.13c}$$

$$\partial_t \phi_{2\Gamma} = -\Gamma_{12} \Big[\boldsymbol{n} \cdot \kappa_1 \nabla \phi_1 - \kappa_{1\Gamma}\Delta_\Gamma \phi_{1\Gamma} + \frac{\partial f_s}{\partial \phi_{1\Gamma}} \Big] - \Gamma_2 \Big[\boldsymbol{n} \cdot \kappa_2 \nabla \phi_2 - \kappa_{2\Gamma}\Delta_\Gamma \phi_{2\Gamma} + \frac{\partial f_s}{\partial \phi_{2\Gamma}} \Big], \tag{2.13d}$$

where Γ_1, Γ_2 and Γ_{12} are the relaxation parameters of the dynamic boundary conditions. $M_i(\phi_1, \phi_2)$ and $M_{12}(\phi_1, \phi_2)$ are defined as

$$M_1(\phi_1, \phi_2) = m_1 \phi_1 (1 - \phi_1 - \phi_2), \tag{2.14}$$

$$M_2(\phi_1, \phi_2) = m_2 \phi_2 (1 - \phi_1 - \phi_2), \tag{2.15}$$

$$M_{12}(\phi_1, \phi_2) = m_{12} \phi_1 \phi_2 (1 - \phi_1 - \phi_2) \tag{2.16}$$

to remove the singularity from the Flory-Huggins free-energy density functions. $M_i(\phi_1, \phi_2)$ and Γ_i, $i = 1, 2$ are the diagonal elements in the mobility matrix, depicting the direct effects of forces on the

corresponding fluxes, while $M_{12}(\phi_1, \phi_2)$ and Γ_{12} are the cross-coupling terms denoting the cross interplay of forces and fluxes. The cross-coupling relaxation rate refers to the rate at which perturbations in one variable are coupled to changes in another variable in the system. We note that our model is an extension of the binary model developed in [27]. Our work provides a general framework that can extend all existing binary mixture models [29–31, 35] with dynamic boundary conditions to a ternary model.

Combining the definition of fluxes derived from the Onsager principle with the conservation law (2.6), we obtain the governing equations of the system as follows:

$$\partial_t \phi_1 = \nabla M_1(\phi_1, \phi_2) \cdot \nabla \mu_1 + \nabla M_{12}(\phi_1, \phi_2) \cdot \nabla \mu_2, \tag{2.17a}$$

$$\partial_t \phi_2 = \nabla M_2(\phi_1, \phi_2) \cdot \nabla \mu_2 + \nabla M_{12}(\phi_1, \phi_2) \cdot \nabla \mu_1, \tag{2.17b}$$

with the following boundary conditions:

$$\partial_t \phi_{1\Gamma} = -\Gamma_1 \Big[\boldsymbol{n} \cdot \kappa_1 \nabla \phi_1 - \kappa_{1\Gamma} \Delta_\Gamma \phi_{1\Gamma} + \frac{\partial f_s}{\partial \phi_{1\Gamma}} \Big] - \Gamma_{12} \Big[\boldsymbol{n} \cdot \kappa_2 \nabla \phi_2 - \kappa_{2\Gamma} \Delta_\Gamma \phi_{2\Gamma} + \frac{\partial f_s}{\partial \phi_{2\Gamma}} \Big], \tag{2.18a}$$

$$\partial_t \phi_{2\Gamma} = -\Gamma_2 \Big[\boldsymbol{n} \cdot \kappa_2 \nabla \phi_2 - \kappa_{2\Gamma} \Delta_\Gamma \phi_{2\Gamma} + \frac{\partial f_s}{\partial \phi_{2\Gamma}} \Big] - \Gamma_{12} \Big[\boldsymbol{n} \cdot \kappa_1 \nabla \phi_1 - \kappa_{1\Gamma} \Delta_\Gamma \phi_{1\Gamma} + \frac{\partial f_s}{\partial \phi_{1\Gamma}} \Big], \tag{2.18b}$$

$$\partial_n \mu_1|_\Gamma = 0, \tag{2.18c}$$

$$\partial_n \mu_2|_\Gamma = 0. \tag{2.18d}$$

We denote the diffusion coefficients as $D_i = m_i k_B T$, $i = 1, 2$, and $D_{12} = m_{12} k_B T$. In this work, we use the dynamic boundary conditions given by (2.18) in the x direction and the periodic boundary condition for all variables in the y direction.

Our model has the following properties:

Theorem 2.1. *The total mass of each component in the domain* Ω *is conserved, i.e.,*

$$\int_\Omega \phi_i(x, y, t) d\boldsymbol{x} = \int_\Omega \phi_i(x, y, 0) d\boldsymbol{x}, \quad i = 1, 2. \tag{2.19}$$

proof: For $i = 1$,

$$\frac{d}{dt} \int_\Omega \phi_1 dx = \int_\Omega \partial_t \phi_1 dx = - \int_\Omega \nabla \cdot \boldsymbol{J_1} dx = \int_\Gamma \boldsymbol{J_1} \cdot \boldsymbol{n} dS$$

$$= \int_\Gamma \Big[- M_1(\phi_1, \phi_2) \nabla \mu_1 - M_{12}(\phi_1, \phi_2) \nabla \mu_2 \Big] \cdot \boldsymbol{n} dS = 0, \tag{2.20}$$

with the boundary conditions $\partial_n \mu_1|_\Gamma = 0$ and $\partial_n \mu_2|_\Gamma = 0$. It is similar for $i = 2$. Thus, (2.19) is obtained.

Theorem 2.2. *The total free energy is dissipative, i.e.,*

$$\partial_t E = \partial_t (E_{\text{surf}} + E_{\text{bulk}}) \le 0. \tag{2.21}$$

proof: For simplicity, we assume that $\nu_1 = \nu_2 = \nu$, and we define

$$\mu_{1\Gamma} = \boldsymbol{n} \cdot \kappa_1 \nabla \phi_1 - \kappa_{1\Gamma} \Delta_\Gamma \phi_{1\Gamma} + \frac{\partial f_s}{\partial \phi_{1\Gamma}}, \tag{2.22}$$

$$\mu_{2\Gamma} = \boldsymbol{n} \cdot \kappa_2 \nabla \phi_2 - \kappa_{2\Gamma} \Delta_\Gamma \phi_{2\Gamma} + \frac{\partial f_s}{\partial \phi_{2\Gamma}}. \tag{2.23}$$

The total energy dissipation rate is given by

$$
\begin{aligned}
\partial_t E &= \int_\Omega dx \Big[(\frac{\partial f_b}{\partial \phi_1} - \kappa_1 \Delta \phi_1) \partial_t \phi_1 + (\frac{\partial f_b}{\partial \phi_2} - \kappa_2 \Delta \phi_2) \partial_t \phi_2 \Big] \\
&\quad + \int_\Gamma dS \Big[\boldsymbol{n} \cdot \kappa_1 \nabla \phi_1 + (\frac{\partial f_s}{\partial \phi_{1\Gamma}} - \kappa_{1\Gamma} \Delta_\Gamma \phi_1) \Big] \frac{\partial \phi_{1\Gamma}}{\partial t} + \int_\Gamma dS \Big[\boldsymbol{n} \cdot \kappa_2 \nabla \phi_2 + (\frac{\partial f_s}{\partial \phi_{2\Gamma}} - \kappa_{2\Gamma} \Delta_\Gamma \phi_2) \Big] \frac{\partial \phi_{2\Gamma}}{\partial t} \\
&= - \int_\Omega dx \frac{1}{\nu} \Big[M_1(\phi_1, \phi_2) |\nabla \mu_1|^2 + 2 M_{12}(\phi_1, \phi_2) \nabla \mu_1 \cdot \nabla \mu_2 + M_2(\phi_1, \phi_2) |\nabla \mu_2|^2 \Big] \\
&\quad - \int_\Gamma dS \Big[\Gamma_1 \mu_{1\Gamma}^2 + 2\Gamma_{12} \mu_{1\Gamma} \mu_{2\Gamma} + \Gamma_2 \mu_{2\Gamma}^2 \Big]. \tag{2.24}
\end{aligned}
$$

Since the mobility matrices $\begin{bmatrix} M_1 & M_{12} \\ M_{12} & M_2 \end{bmatrix}$, $\begin{bmatrix} \Gamma_1 & \Gamma_{12} \\ \Gamma_{12} & \Gamma_2 \end{bmatrix}$ are positive definite, $\partial_t E \le 0$ holds.

2.2. Non-dimensionalization

We set the characteristic length scale as the molecular length $l_0 = \nu^{1/3}$ and characteristic timescale $t_0 = \nu^{2/3}/D_1$ such that $\tilde{D}_1 = D_1 t_0 / l_0^2 = 1$. Rescaling $\tilde{\boldsymbol{x}} = \boldsymbol{x}/l_0$ and $\tilde{t} = t/t_0$, our model has the following non-dimensional parameters:

$$\tilde{D}_2 = \frac{D_2}{D_1}, \quad \tilde{D}_{12} = \frac{D_{12}}{D_1}, \quad \tilde{\Gamma}_i = \Gamma_i \frac{k_B T}{\nu_s} t_0, \quad \bar{\kappa}_i = \kappa_i \frac{\nu_s}{k_B T} \frac{1}{l_0} = \frac{\nu^{1/3}}{l_0}, \tag{2.25}$$

$$\tilde{f}_s = f_s \frac{\nu_s}{k_B T}, \quad \tilde{\kappa}_{i\Gamma} = \frac{1}{l_0^{2/3}} \kappa_{i\Gamma} \frac{\nu_s}{k_B T}, \quad \tilde{\kappa}_i = \frac{1}{l_0^{2/3}} \kappa_i \frac{\nu}{k_B T}, i = 1, 2. \tag{2.26}$$

For brevity, we skip the tildes in the following equations. The dimensionless equations governing the kinetics of the system are given as

$$\partial_t \phi_1 = \nabla \phi_1 (1 - \phi_1 - \phi_2) \cdot \nabla \mu_1 + \nabla D_{12} \phi_1 \phi_2 (1 - \phi_1 - \phi_2) \cdot \nabla \mu_2, \tag{2.27a}$$

$$\partial_t \phi_2 = \nabla D_{12} \phi_1 \phi_2 (1 - \phi_1 - \phi_2) \cdot \nabla \mu_1 + \nabla D_2 \phi_2 (1 - \phi_1 - \phi_2) \cdot \nabla \mu_2, \tag{2.27b}$$

with the dimensionless boundary conditions written as

$$\partial_t \phi_{1\Gamma} = -\Gamma_1 \Big[\boldsymbol{n} \cdot \bar{\kappa}_1 \nabla \phi_1 - \kappa_{1\Gamma} \Delta_\Gamma \phi_{1\Gamma} + \frac{\partial f_s}{\partial \phi_{1\Gamma}} \Big] - \Gamma_{12} \Big[\boldsymbol{n} \cdot \bar{\kappa}_2 \nabla \phi_2 - \kappa_{2\Gamma} \Delta_\Gamma \phi_{2\Gamma} + \frac{\partial f_s}{\partial \phi_{2\Gamma}} \Big], \tag{2.28a}$$

$$\partial_t \phi_{2\Gamma} = -\Gamma_2 \Big[\boldsymbol{n} \cdot \bar{\kappa}_2 \nabla \phi_2 - \kappa_{2\Gamma} \Delta_\Gamma \phi_{2\Gamma} + \frac{\partial f_s}{\partial \phi_{2\Gamma}} \Big] - \Gamma_{12} \Big[\boldsymbol{n} \cdot \bar{\kappa}_1 \nabla \phi_1 - \kappa_{1\Gamma} \Delta_\Gamma \phi_{1\Gamma} + \frac{\partial f_s}{\partial \phi_{1\Gamma}} \Big], \tag{2.28b}$$

$$\partial_{\boldsymbol{n}} \mu_1 |_\Gamma = 0, \tag{2.28c}$$

$$\partial_{\boldsymbol{n}} \mu_2 |_\Gamma = 0. \tag{2.28d}$$

In the next section, we will develop the numerical scheme based on the IEQ method [51–53].

3. Numerical scheme

We first reformulate the mathematical model into an equivalent form. Then, we discretize the reformulated system in time and space, respectively. In this work, we consider the 2D domain for simplicity.

3.1. Mathematical reformulation

We reformulate the total free energy in a quadratic form:

$$q_1 = \sqrt{\frac{\phi_1}{n_1}\ln\phi_1 + \frac{\phi_2}{n_2}\ln\phi_2 + (1 - \phi_1 - \phi_2)\ln(1 - \phi_1 - \phi_2) + \chi_{12}\phi_1\phi_2 + \chi_{13}\phi_1\phi_3 + \chi_{23}\phi_2\phi_3 + C}, \quad (3.1)$$

where C is a constant such that the value under the square root is positive; $\phi_3 = 1 - \phi_1 - \phi_2$. Then, the total energy becomes

$$E = E_{\text{surf}} + E_{\text{bulk}} = E_{\text{surf}} + \int_\Omega \left[q_1^2 + \omega_1\phi_1 + \omega_2\phi_2 + \frac{\kappa_1}{2}|\nabla\phi_1|^2 + \frac{\kappa_2}{2}|\nabla\phi_2|^2 \right] dx; \quad (3.2)$$

the chemical potentials become

$$\mu_1 = 2q_1\frac{\partial q_1}{\partial\phi_1} + \omega_1 - \kappa_1\Delta\phi_1, \quad (3.3a)$$

$$\mu_2 = 2q_1\frac{\partial q_1}{\partial\phi_2} + \omega_2 - \kappa_2\Delta\phi_2. \quad (3.3b)$$

The reformulated governing equations of the system are as follows:

$$\partial_t\phi_1 = \nabla M_1(\phi_1, \phi_2)\cdot\nabla\mu_1 + \nabla M_{12}(\phi_1, \phi_2)\cdot\nabla\mu_2, \quad (3.4a)$$

$$\partial_t\phi_2 = \nabla M_2(\phi_1, \phi_2)\cdot\nabla\mu_2 + \nabla M_{12}(\phi_1, \phi_2)\cdot\nabla\mu_1, \quad (3.4b)$$

$$\partial_t q_1 = \frac{\partial q_1}{\partial\phi_1}\partial_t\phi_1 + \frac{\partial q_1}{\partial\phi_2}\partial_t\phi_2, \quad (3.4c)$$

with the following boundary conditions:

$$\partial_t\phi_{1\Gamma} = -\Gamma_1\left[\boldsymbol{n}\cdot\kappa_1\nabla\phi_1 - \kappa_{1\Gamma}\Delta_\Gamma\phi_{1\Gamma} + \frac{\partial f_s}{\partial\phi_{1\Gamma}} \right] - \Gamma_{12}\left[\boldsymbol{n}\cdot\kappa_2\nabla\phi_2 - \kappa_{1\Gamma}\Delta_\Gamma\phi_{2\Gamma} + \frac{\partial f_s}{\partial\phi_{2\Gamma}} \right], \quad (3.5a)$$

$$\partial_t\phi_{2\Gamma} = -\Gamma_2\left[\boldsymbol{n}\cdot\kappa_2\nabla\phi_2 - \kappa_{1\Gamma}\Delta_\Gamma\phi_{2\Gamma} + \frac{\partial f_s}{\partial\phi_{2\Gamma}} \right] - \Gamma_{12}\left[\boldsymbol{n}\cdot\kappa_1\nabla\phi_1 - \kappa_{1\Gamma}\Delta_\Gamma\phi_{1\Gamma} + \frac{\partial f_s}{\partial\phi_{1\Gamma}} \right], \quad (3.5b)$$

$$\partial_n\mu_1|_\Gamma = 0, \quad (3.5c)$$

$$\partial_n\mu_2|_\Gamma = 0. \quad (3.5d)$$

The reformulated system has the following properties.

Theorem 3.1. *The total mass of each component in the domain Ω is conserved, i.e.,*

$$\int_\Omega \phi_i(x, y, t)dx = \int_\Omega \phi_i(x, y, 0)dx, \quad i = 1, 2. \quad (3.6)$$

Theorem 3.2. *The total free energy is dissipative, i.e.,*

$$\partial_t E = \partial_t(E_{\text{surf}} + E_{\text{bulk}}) \le 0. \tag{3.7}$$

We skip the proof here. Next, we will discretize the reformulated governing equation in both the time and space directions.

3.2. Semi-discrete scheme in time

We use the Crank-Nicolson method in the time direction. Δt is the time step. $(\cdot)^n$ represents the solution at the nth time step, i.e., $t_n = n\Delta t$. We denote

$$\partial_t^{n+1}(\cdot) = \frac{(\cdot)^{n+1} - (\cdot)^n}{\Delta t}, \quad (\cdot)^{n+1/2} = \frac{(\cdot)^n + (\cdot)^{n+1}}{2}, \quad (\bar{\cdot})^{n+1/2} = \frac{3(\cdot)^n - (\cdot)^{n-1}}{2}. \tag{3.8}$$

The governing equations of the system are as follows:

$$\partial_t^{n+1}\phi_1 = \nabla M_1(\bar{\phi}_1^{\,n+1/2}, \bar{\phi}_2^{\,n+1/2}) \cdot \nabla \mu_1^{n+1/2} + \nabla M_{12}(\bar{\phi}_1^{\,n+1/2}, \bar{\phi}_2^{\,n+1/2}) \cdot \nabla \mu_2^{n+1/2}, \tag{3.9a}$$

$$\partial_t^{n+1}\phi_2 = \nabla M_2(\bar{\phi}_1^{\,n+1/2}, \bar{\phi}_2^{\,n+1/2}) \cdot \nabla \mu_2^{n+1/2} + \nabla M_{12}(\bar{\phi}_1^{\,n+1/2}, \bar{\phi}_2^{\,n+1/2}) \cdot \nabla \mu_1^{n+1/2}, \tag{3.9b}$$

$$\partial_t^{n+1}q_1 = \frac{\partial \bar{q}_1}{\partial \phi_1}^{n+1/2} \partial_t^{n+1}\phi_1 + \frac{\partial \bar{q}_1}{\partial \phi_2}^{n+1/2} \partial_t^{n+1}\phi_2, \tag{3.9c}$$

with the following boundary conditions:

$$\partial_t^{n+1}\phi_{1\Gamma} = -\Gamma_1 \Big[\boldsymbol{n} \cdot \bar{\kappa}_1 \nabla \phi_1^{n+1/2} - \kappa_{1\Gamma}\Delta_\Gamma \phi_{1\Gamma}^{n+1/2} + \frac{\partial f_s}{\partial \phi_{1\Gamma}}^{n+1/2} \Big] \tag{3.10a}$$

$$\qquad - \Gamma_{12} \Big[\boldsymbol{n} \cdot \bar{\kappa}_2 \nabla \phi_2^{n+1/2} - \kappa_{1\Gamma}\Delta_\Gamma \phi_{2\Gamma}^{n+1/2} + \frac{\partial f_s}{\partial \phi_{2\Gamma}}^{n+1/2} \Big],$$

$$\partial_t^{n+1}\phi_{2\Gamma} = -\Gamma_2 \Big[\boldsymbol{n} \cdot \bar{\kappa}_2 \nabla \phi_2^{n+1/2} - \kappa_{1\Gamma}\Delta_\Gamma \phi_{2\Gamma}^{n+1/2} + \frac{\partial f_s}{\partial \phi_{2\Gamma}}^{n+1/2} \Big] \tag{3.10b}$$

$$\qquad - \Gamma_{12} \Big[\boldsymbol{n} \cdot \bar{\kappa}_1 \nabla \phi_1^{n+1/2} - \kappa_{1\Gamma}\Delta_\Gamma \phi_{1\Gamma}^{n+1/2} + \frac{\partial f_s}{\partial \phi_{1\Gamma}}^{n+1/2} \Big],$$

$$\partial_n \mu_1^{n+1}|_\Gamma = 0, \tag{3.10c}$$
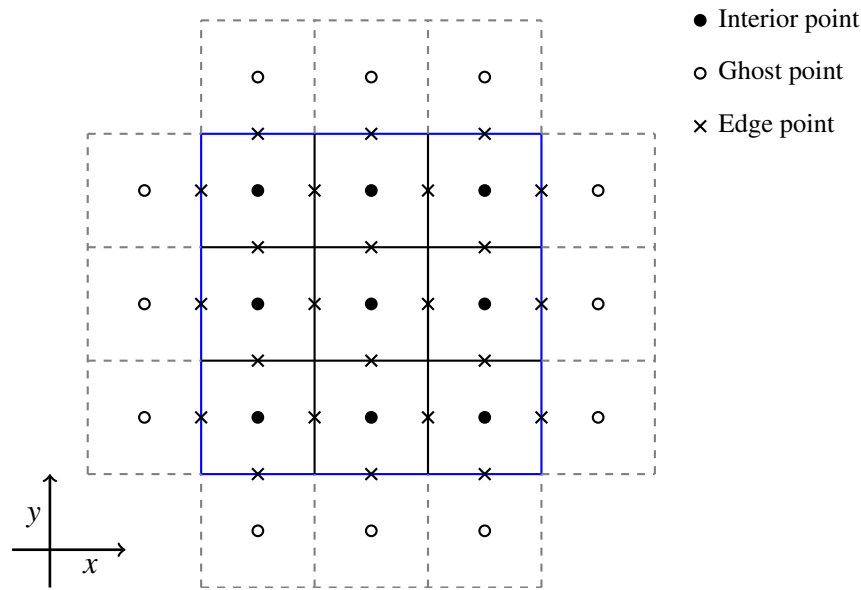
$$\partial_n \mu_2^{n+1}|_\Gamma = 0, \tag{3.10d}$$

where

$$\mu_1^{n+1/2} = 2q_1^{n+1/2}\frac{\partial \bar{q}_1}{\partial \phi_1}^{n+1/2} + \omega_1 - \kappa_1 \Delta \phi_1^{n+1/2}, \tag{3.11a}$$

$$\mu_2^{n+1/2} = 2q_1^{n+1/2}\frac{\partial \bar{q}_1}{\partial \phi_2}^{n+1/2} + \omega_2 - \kappa_2 \Delta \phi_2^{n+1/2}. \tag{3.11b}$$

3.3. Fully discrete scheme

We use the central finite-difference method such that there is second-order accuracy in the space. Specifically, we apply a uniform mesh in 2D space $[0, L] \times [0, L]$ (see Figure 1). In the x direction, the

Figure 1. Sketch of the staggered mesh in 2D space. The blue line is the boundary Γ of the 2D domain $\Omega = [0, L] \times [0, L]$ in the $x - y$ plane. The black solid points are the center points inside the bulk, the black empty points are the ghost points adjacent to the boundary Γ and the crosses denote the edge points.

domain is divided into N_x equal-sized subintervals. Similarly, in the y direction, the domain is divided into N_y subintervals, each of equal size. We discretize the scalar functions given as ϕ_i and $\Delta\phi_i$ values at the center point (x_i, y_j), where

$$x_i = \left(i - \frac{1}{2}\right)\frac{L}{N_x}, \qquad i = 0, 1, \cdots, N_x + 1, \tag{3.12}$$

$$y_j = \left(j - \frac{1}{2}\right)\frac{L}{N_y}, \qquad j = 0, 1, \cdots, N_y + 1, \tag{3.13}$$

and we discretize the vector functions, e.g., $\nabla\phi_i$, at the edge points $(x_{i+\frac{1}{2}}, y_j)$ or $(x_i, y_{j+\frac{1}{2}})$ [55], where

$$x_{i+\frac{1}{2}} = i\frac{L}{N_x}, \qquad i = 0, 1, \cdots, N_x, \tag{3.14}$$

$$y_{j+\frac{1}{2}} = j\frac{L}{N_y}, \qquad j = 0, 1, \cdots, N_y. \tag{3.15}$$

At the boundary Γ, we use the average value at adjacent discrete center points, e.g.,

$$\phi_{1\Gamma}^n|_{\frac{1}{2},j} = \frac{\phi_1^n|_{0,j} + \phi_1^n|_{1,j}}{2}, \qquad \phi_{1\Gamma}^n|_{N_x+\frac{1}{2},j} = \frac{\phi_1^n|_{N_x,j} + \phi_1^n|_{N_x+1,j}}{2}, \tag{3.16}$$

$j = 1, \cdots N_y$, is the index in the y direction.

We respectively denote the edge-to-center average and difference operator as a_x and d_x in the x direction and a_y and d_y in the y direction, which are defined as follows:

$$a_x u_{i,j} := \frac{1}{2}(u_{i+\frac{1}{2},j} + u_{i-\frac{1}{2},j}), \quad d_x u_{i,j} := \frac{1}{h_x}(u_{i+\frac{1}{2},j} - u_{i-\frac{1}{2},j}), \tag{3.17}$$

$$a_y v_{i,j} := \frac{1}{2}(v_{i,j+\frac{1}{2}} + v_{i,j-\frac{1}{2}}), \quad d_y u_{i,j} := \frac{1}{h_y}(v_{i,j+\frac{1}{2}} - v_{i,j-\frac{1}{2}}). \tag{3.18}$$
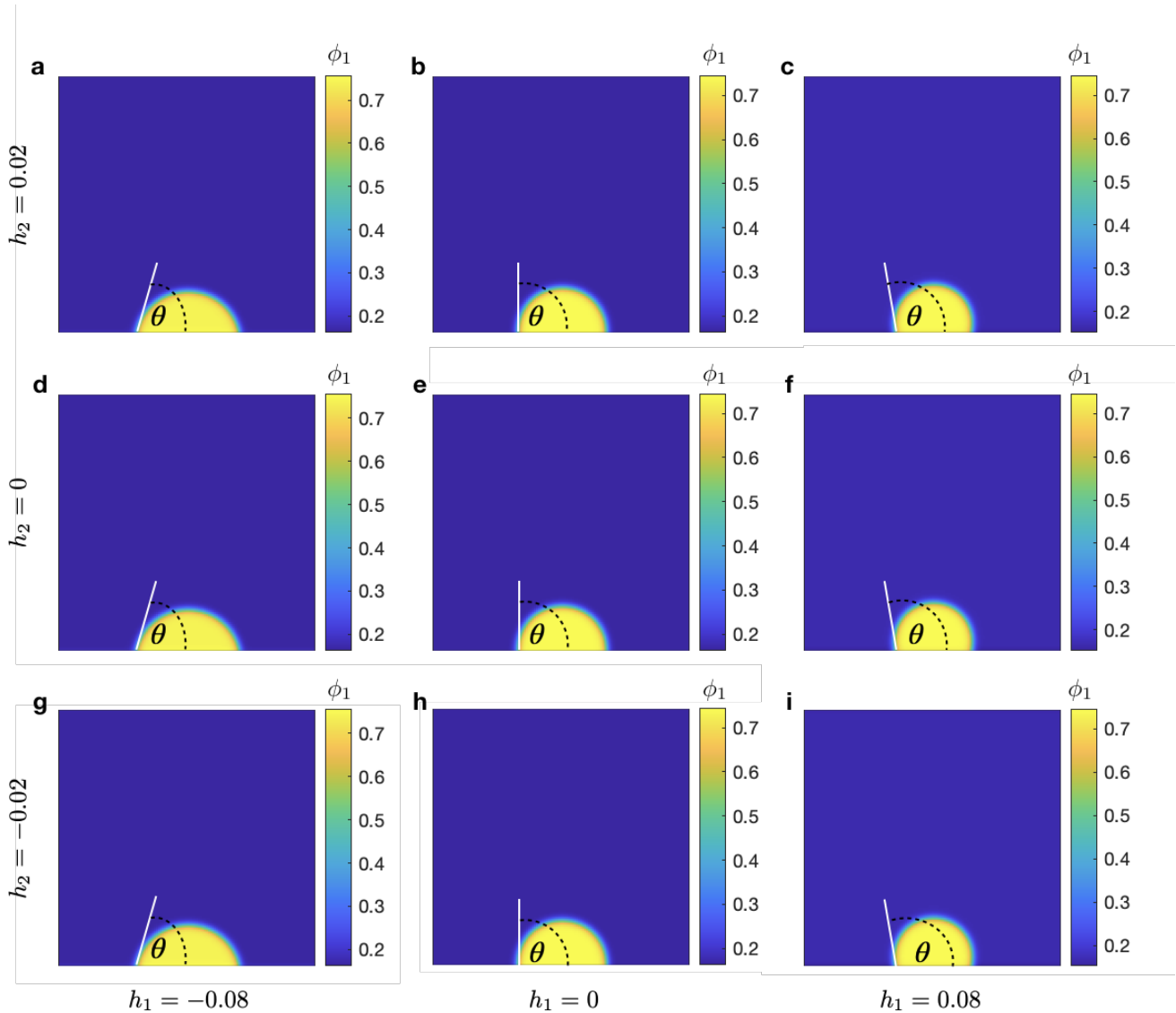
Figure 2. Profiles of ϕ_1 with a linear interaction between solid walls and mixture components along the contact angle of a two-phase coexisting mixture in equilibrium. The snapshots denote the profiles of component 1, i.e., ϕ_1, with different values of h_1 and h_2. At each snapshot, the yellow area depicts the condensates and a white line is used to denote the tangent line of the spherical interface at the contact point on the surface Γ. The contact angle of a droplet between the tangent line and surface is denoted by θ. In each column (row), we use the same h_1 (h_2) values. The basic parameter values used in this case are as follows: $\kappa_{1\Gamma} = \kappa_{2\Gamma} = 0$, $\kappa_1 = \kappa_2 = 1$, $g_1 = g_2 = \gamma = 0$, $\chi_{12} = -1$, $\chi_{23} = 0$, $\chi_{13} = 2.5$. Since the droplet is a composite of ϕ_1, mainly, and the contact angle is determined by the value of h_1 in this study.
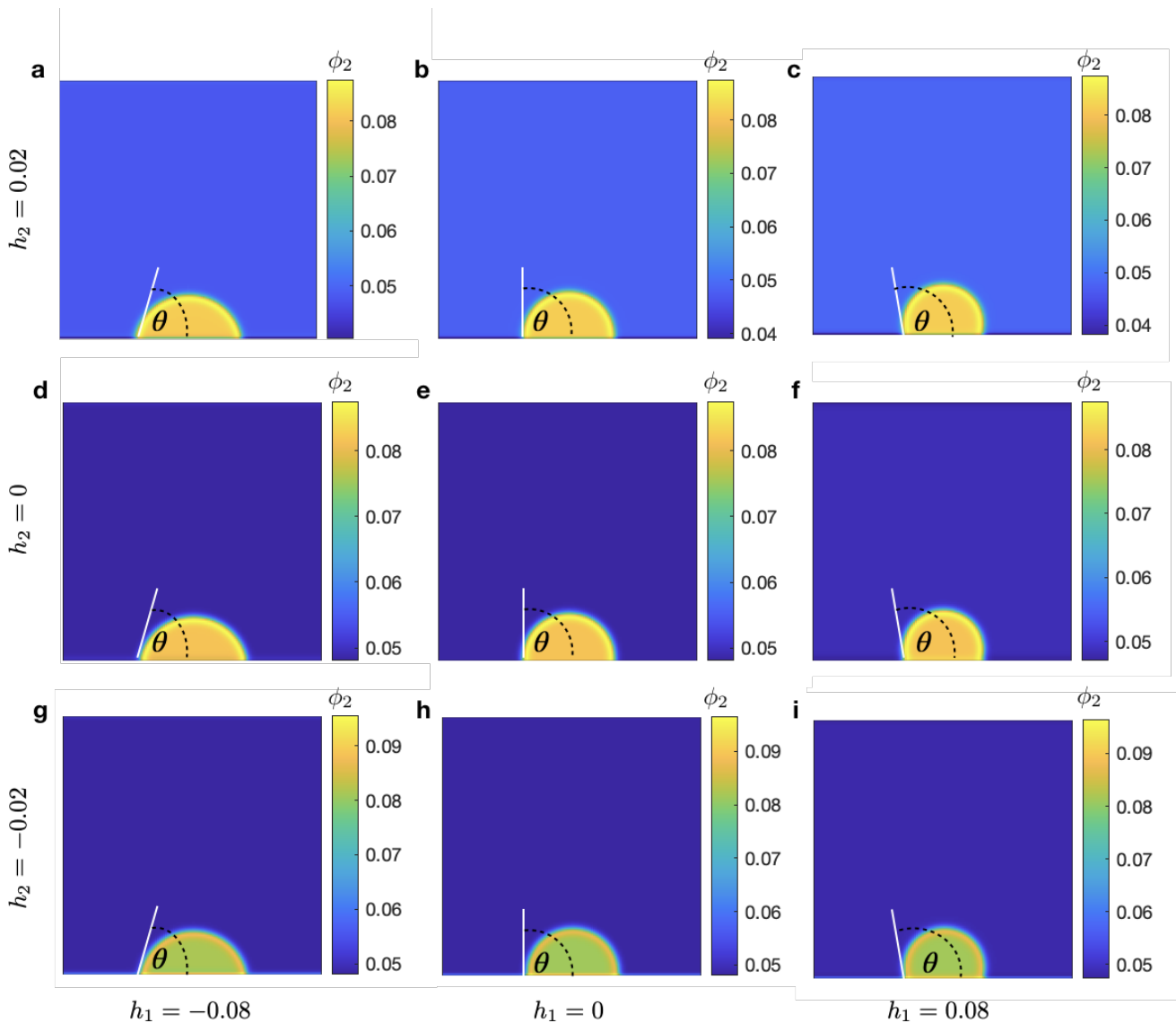
Figure 3. Profiles of ϕ_2 with a linear interaction between solid walls and mixture components along the contact angle of a two-phase coexisting mixture in equilibrium. The snapshots denote the profiles of component 2, i.e., ϕ_2, with different values of h_1 and h_2. The profile of ϕ_2 changes rapidly near the surface with respect to different h_2 values. However, the contact angle is determined by the value of h_1 since the the droplet mainly contains ϕ_1. The basic parameter values used in this case are as follows: $\kappa_{1\Gamma} = \kappa_{2\Gamma} = 0$, $\kappa_1 = \kappa_2 = 1$, $g_1 = g_2 = \gamma = 0$, $\chi_{12} = -1, \chi_{23} = 0, \chi_{13} = 2.5$.

We respectively denote the center-to-edge average and difference operators by A_x and D_x in the x direction. Analogously, the center-to-edge average in the y direction and difference operators are respectively denoted as A_y and D_y. Their definitions are as follows:

$$A_x\phi_{i+\frac{1}{2},j} := \frac{1}{2}(\phi_{i+1,j} + \phi_{i,j}), \quad D_x\phi_{i+\frac{1}{2},j} := \frac{1}{h_x}(\phi_{i+1,j} - \phi_{i,j}), \tag{3.19}$$

$$A_y\phi_{i,j+\frac{1}{2}} := \frac{1}{2}(\phi_{i,j+1} + \phi_{i,j}), \quad D_y\phi_{i,j+\frac{1}{2}} := \frac{1}{h_y}(\phi_{i,j+1} - \phi_{i,j}). \tag{3.20}$$

The standard 2D discrete Laplace operator is defined as Δ_h in the bulk and $\Delta_{\Gamma h}$ on the surface.

$$\Delta_h\phi := d_x(D_x\phi) + d_y(D_y\phi), \quad \Delta_{\Gamma h}\phi_\Gamma := d_y(D_y\phi_\Gamma), \quad \text{or} \quad \Delta_{\Gamma h}\phi_\Gamma := d_x(D_x\phi_\Gamma). \tag{3.21}$$
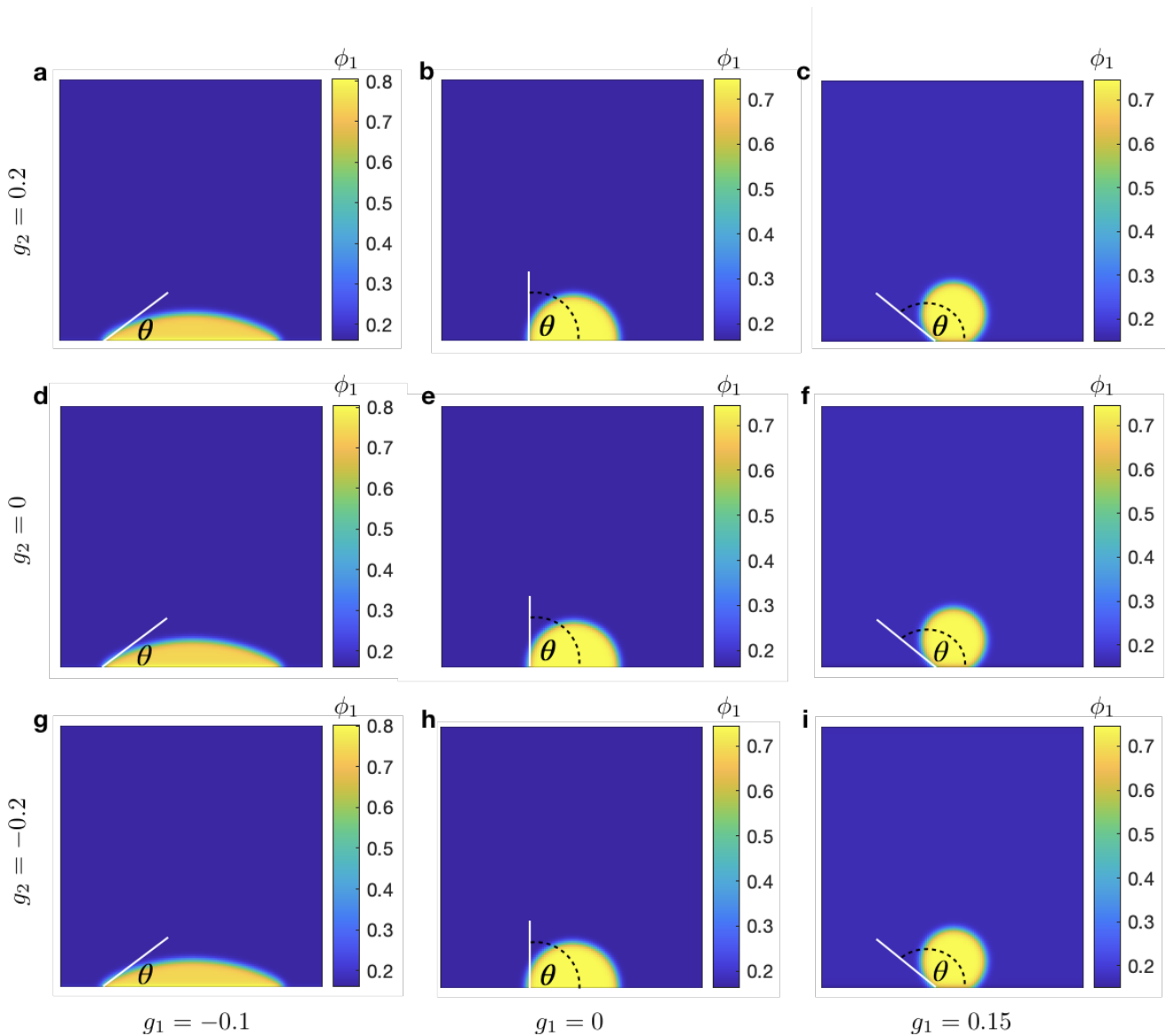
Figure 4. Profiles of ϕ_1 with a quadratic interaction between solid walls and mixture components along the contact angle of a two-phase coexisting mixture in equilibrium. The snapshots denote the profiles of component 1, i.e., ϕ_1, with different values of g_1 and g_2. We observe that the interaction between ϕ_2 and a solid wall mainly influences the contact angle. The basic parameter values used in this case are as follows: $\kappa_{1\Gamma} = \kappa_{2\Gamma} = 0$, $\kappa_1 = \kappa_2 = 0$, $h_1 = h_2 = \gamma = 0, \chi_{12} = -1, \chi_{23} = 0, \chi_{13} = 2.5$.

The discrete norm in the bulk and surface are defined as follows:

$$\|\phi\|_c = h_x h_y \sum_{i=1}^{N_x} \sum_{j=1}^{N_y} \phi_{i,j}, \qquad \|\nabla\phi\|_v = h_x h_y \sum_{i=1}^{N_x} \sum_{j=1}^{N_y} \Big[a_x D_x \phi_{i+1/2,j} + a_y D_y \phi_{i,j+1/2} \Big], \qquad (3.22)$$

$$\|\phi\|_{c,\Gamma} = h_y \sum_{j=1}^{N_y} \phi_{j\Gamma}, \qquad \|\nabla\phi\|_{v,\Gamma} = h_y \sum_{j=1}^{N_y} \Big[a_y D_y \phi_{i,j+1/2} \Big]. \qquad (3.23)$$

The fully discrete numerical scheme:

$$\Big\{ \partial_t^{n+1} \phi_1 = d_x A_x (M_1(\bar{\phi}_1^{\,n+1/2}, \bar{\phi}_2^{\,n+1/2}) D_x \mu_1^{n+1/2} + d_y A_y (M_1(\bar{\phi}_1^{\,n+1/2}, \bar{\phi}_2^{\,n+1/2})) D_y \mu_1^{n+1/2}$$
$$+ d_x A_x (M_{12}(\bar{\phi}_1^{\,n+1/2}, \bar{\phi}_2^{\,n+1/2}) D_x \mu_2^{n+1/2} + d_y A_y (M_{12}(\bar{\phi}_1^{\,n+1/2}, \bar{\phi}_2^{\,n+1/2})) D_y \mu_2^{n+1/2} \Big\}\Big|_{i,j}, \qquad (3.24)$$

$$\Big\{ \partial_t^{n+1} \phi_2 = d_x A_x (M_2(\bar{\phi}_1^{\,n+1/2}, \bar{\phi}_2^{\,n+1/2}) D_x \mu_2^{n+1/2} + d_y A_y (M_2(\bar{\phi}_1^{\,n+1/2}, \bar{\phi}_2^{\,n+1/2})) D_y \mu_2^{n+1/2}$$
$$+ d_x A_x (M_{12}(\bar{\phi}_1^{\,n+1/2}, \bar{\phi}_2^{\,n+1/2}) D_x \mu_1^{n+1/2} + d_y A_y (M_{12}(\bar{\phi}_1^{\,n+1/2}, \bar{\phi}_2^{\,n+1/2})) D_y \mu_1^{n+1/2} \Big\}\Big|_{i,j}, \qquad (3.25)$$

$$\Big\{ \partial_t^{n+1} q_1 = \frac{\overline{\partial q_1}}{\partial \phi_1}^{\,n+1/2} \partial_t^{n+1} \phi_1 + \frac{\overline{\partial q_1}}{\partial \phi_2}^{\,n+1/2} \partial_t^{n+1} \phi_2 \Big\}\Big|_{i,j}, \qquad (3.26)$$

where $i = 1, \cdots N_x$, $j = 1, \cdots N_y$, with the following boundary conditions:

$$\Big\{ \partial_t^{n+1} \phi_{1\Gamma} = -\Gamma_1 \Big[\boldsymbol{n} \cdot \bar{\kappa}_1 d_x \phi_1^{n+1/2} - \kappa_{1\Gamma} \Delta_{\Gamma h} \phi_{1\Gamma}^{n+1/2} + \frac{\partial f_s}{\partial \phi_{1\Gamma}}^{\,n+1/2} \Big] \qquad (3.27a)$$
$$- \Gamma_{12} \Big[\boldsymbol{n} \cdot \bar{\kappa}_2 d_x \phi_2^{n+1/2} - \kappa_{2\Gamma} \Delta_{\Gamma h} \phi_{2\Gamma}^{n+1/2} + \frac{\partial f_s}{\partial \phi_{2\Gamma}}^{\,n+1/2} \Big] \Big\}\Big|_{\frac{1}{2} \text{or}(N_x + \frac{1}{2}),j},$$

$$\Big\{ \partial_t^{n+1} \phi_{2\Gamma} = -\Gamma_2 \Big[\boldsymbol{n} \cdot \bar{\kappa}_2 d_x \phi_2^{n+1/2} - \kappa_{2\Gamma} \Delta_{\Gamma h} \phi_{2\Gamma}^{n+1/2} + \frac{\partial f_s}{\partial \phi_{2\Gamma}}^{\,n+1/2} \Big] \qquad (3.27b)$$
$$- \Gamma_{12} \Big[\boldsymbol{n} \cdot \bar{\kappa}_1 d_x \phi_1^{n+1/2} - \kappa_{1\Gamma} \Delta_{\Gamma h} \phi_{1\Gamma}^{n+1/2} + \frac{\partial f_s}{\partial \phi_{1\Gamma}}^{\,n+1/2} \Big] \Big\}\Big|_{\frac{1}{2} \text{or}(N_x + \frac{1}{2}),j},$$

$$\mu_k|_{0,j} = \mu_k|_{1,j}, \qquad \mu_k|_{N_x,j} = \mu_k|_{N_x+1,j}, \qquad k = 1, 2. \qquad (3.27c)$$
$$\mu_k|_{i,0} = \mu_k|_{i,1}, \qquad \mu_k|_{i,N_y} = \mu_k|_{i,N_y+1}, \qquad k = 1, 2, \qquad (3.27d)$$

where

$$\mu_1^{n+1/2}|_{i,j} = 2q_1|_{i,j}^{n+1/2} \frac{\overline{\partial q_1}}{\partial \phi_1}^{\,n+1/2}|_{i,j} + \omega_1 - \kappa_1 \Delta_h \phi_1^{n+1/2}|_{i,j}, \qquad (3.28a)$$

$$\mu_2^{n+1/2}|_{i,j} = 2q_1|_{i,j}^{n+1/2} \frac{\overline{\partial q_1}}{\partial \phi_2}^{\,n+1/2}|_{i,j} + \omega_2 - \kappa_2 \Delta_h \phi_2^{n+1/2}|_{i,j}. \qquad (3.28b)$$
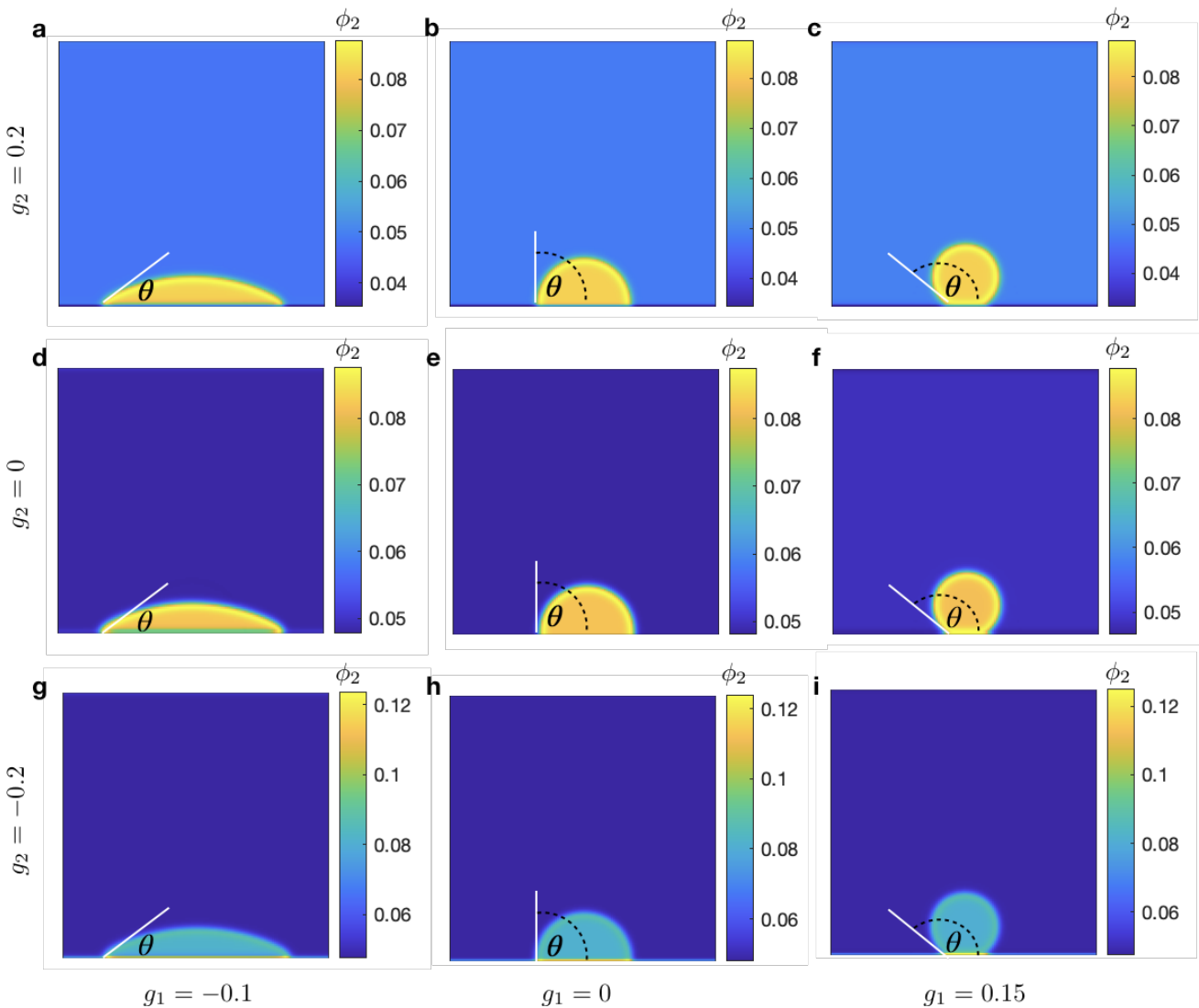
The fully discrete numerical scheme satisfies the conditions of the total mass conservation law and the total energy dissipation rate at the discrete level.

Theorem 3.3. *Mass conservation law at discrete level:* *Based on the discrete boundary conditions given by* (3.27),

$$\sum_{i=1}^{N_x} \sum_{j=1}^{N_y} \frac{\phi_1^{n+1}|_{i,j} - \phi_1^n|_{i,j}}{\Delta t} = \sum_{i=1}^{N_x} \sum_{j=1}^{N_y} \left[\nabla \cdot M_1 \nabla \mu_1^{n+1/2}|_{i,j} + \nabla \cdot M_{12} \nabla \mu_2^{n+1/2}|_{i,j} \right] = 0; \quad (3.29)$$

it is the same as for the total mass of ϕ_2.

Figure 5. Profiles of ϕ_2 with a quadratic interaction between solid walls and mixture components along the contact angle of a two-phase coexisting mixture in equilibrium. The snapshots denote the profiles of component 2, i.e., ϕ_2, with different values of g_1 and g_2. We find that the interaction between ϕ_1 and a solid surface changes the profiles of ϕ_2 near the surface, while the contact angle is determined by the interaction between ϕ_1 and a solid wall. The basic parameter values used in this case are as follows: $\kappa_{1\Gamma} = \kappa_{2\Gamma} = 0$, $\kappa_1 = \kappa_2 = 1$, $h_1 = h_2 = \gamma = 0$, $\chi_{12} = -1$, $\chi_{23} = 0$, $\chi_{13} = 2.5$.

Theorem 3.4. *Unconditional energy stability at discrete level:* *The discrete energy of the system is defined as*

$$E^{n+1} = E^{n+1}_{\text{bulk}} + E^{n+1}_{\text{surf}}, \tag{3.30}$$

where

$$E^{n+1}_{\text{bulk}} = \|f_b(\phi_1, \phi_2)^{n+1}\|_c + \frac{\kappa_1}{2}\|\nabla\phi_1^{n+1}\|_v^2 + \frac{\kappa_2}{2}\|\nabla\phi_2^{n+1}\|_v^2, \tag{3.31}$$

$$E^{n+1}_{\text{surf}} = \|f_s(\phi_{1\Gamma}, \phi_{2\Gamma})^{n+1}\|_{c,\Gamma} + \frac{\kappa_{1\Gamma}}{2}\|\nabla\phi_{1\Gamma}^{n+1}\|_{v,\Gamma}^2 + \frac{\kappa_{2\Gamma}}{2}\|\nabla\phi_{2\Gamma}^{n+1}\|_{v,\Gamma}^2. \tag{3.32}$$

The total energy at the discrete level decreases with respect to time, i.e.,

$$E^{n+1} \le E^n. \tag{3.33}$$

proof: Using the definition of reformulated total energy at the discrete level given by (3.30) and the formula $(a^2 - b^2) = (a + b)(a - b)$, we obtain

$$
\begin{aligned}
\frac{E^{n+1} - E^n}{\Delta t} =& \left\|2 \cdot \frac{q_1^{n+1} - q_1^n}{\Delta t} \frac{q_1^{n+1} + q_1^n}{2} + \omega_1 \frac{\phi_1^{n+1} - \phi_1^n}{\Delta t} + \omega_2 \frac{\phi_2^{n+1} - \phi_2^n}{\Delta t}\right\|_c \\
&+ \frac{\kappa_1}{2}\left\|2 \cdot \frac{\nabla\phi_1^{n+1} - \nabla\phi_1^n}{\Delta t} \frac{\nabla\phi_1^{n+1} + \nabla\phi_1^n}{2}\right\|_v + \frac{\kappa_2}{2}\left\|2 \cdot \frac{\nabla\phi_2^{n+1} - \nabla\phi_2^n}{\Delta t} \frac{\nabla\phi_2^{n+1} + \nabla\phi_2^n}{2}\right\|_v \\
&+ \frac{\kappa_{1\Gamma}}{2}\left\|2 \cdot \frac{\nabla_\|\phi_{1\Gamma}^{n+1} - \nabla_\|\phi_{1\Gamma}^n}{\Delta t} \frac{\nabla_\|\phi_{1\Gamma}^{n+1} + \nabla_\|\phi_{1\Gamma}^n}{2}\right\|_{v,\Gamma} \\
&+ \frac{\kappa_{2\Gamma}}{2}\left\|2 \cdot \frac{\nabla_\|\phi_{2\Gamma}^{n+1} - \nabla_\|\phi_{2\Gamma}^n}{\Delta t} \frac{\nabla_\|\phi_{2\Gamma}^{n+1} + \nabla_\|\phi_{2\Gamma}^n}{2}\right\|_{v,\Gamma} \\
&+ h_1\left\|\frac{\phi_1^{n+1} - \phi_1^n}{\Delta t}\right\|_c + g_1\left\|2 \cdot \frac{\phi_1^{n+1} - \phi_1^n}{\Delta t} \frac{\phi_1^{n+1} + \phi_1^n}{2}\right\|_c \\
&+ h_2\left\|\frac{\phi_2^{n+1} - \phi_2^n}{\Delta t}\right\|_c + g_2\left\|\frac{\phi_2^{n+1} - \phi_2^n}{\Delta t} \frac{\phi_2^{n+1} + \phi_2^n}{2}\right\|_c \\
&+ \gamma\left\|\frac{\phi_1^{n+1} + \phi_1^n}{2} \frac{\phi_2^{n+1} - \phi_2^n}{\Delta t}\right\|_c + \gamma\left\|\frac{\phi_2^{n+1} + \phi_2^n}{2} \frac{\phi_1^{n+1} - \phi_1^n}{\Delta t}\right\|_c. \tag{3.34}
\end{aligned}
$$

According to the discrete chemical potentials defined in (3.28) and discrete boundary conditions given by (3.27), we have

$$
\begin{aligned}
\frac{E^{n+1} - E^n}{\Delta t} =& \|\mu_1^{n+1/2} \cdot (\nabla M_1 \cdot \nabla\mu_1^{n+1/2} + \nabla M_{12} \cdot \nabla\mu_2^{n+1/2})\|_v \\
&+ \|\mu_2^{n+1/2} \cdot (\nabla M_2 \cdot \nabla\mu_2^{n+1/2} + \nabla M_{12} \cdot \nabla\mu_1^{n+1/2})\|_v \\
&+ \|\mu_{1\Gamma}^{n+1/2} \cdot (-\Gamma_1\mu_{1\Gamma}^{n+1/2} - \Gamma_{12}\mu_{2\Gamma}^{n+1/2})\|_{v,\Gamma} \\
&+ \|\mu_{2\Gamma}^{n+1/2} \cdot (-\Gamma_2\mu_{2\Gamma}^{n+1/2} - \Gamma_{12}\mu_{1\Gamma}^{n+1/2})\|_{v,\Gamma} \\
=& -\|M_1|\nabla\mu_1^{n+1/2}|^2 + 2M_{12}\nabla\mu_1^{n+1/2} \cdot \nabla\mu_2^{n+1/2} + M_2|\nabla\mu_2^{n+1/2}|^2\|_v \\
&- \|\Gamma_1|\mu_{1\Gamma}^{n+1/2}|^2 + 2\Gamma_{12}\mu_{1\Gamma}^{n+1/2}\mu_{2\Gamma}^{n+1/2} + \Gamma_2|\mu_{2\Gamma}^{n+1/2}|^2\|_{v,\Gamma}^2 \le 0, \tag{3.35}
\end{aligned}
$$

i.e., (3.33) is obtained.

4. Physical phenomenon investigation by numerical simulations

Taking advantage of the ability to vary parameters in a controlled manner and over a wide range of scales in numerical simulations, we investigate several physical phenomena in this section, including the wettability of multi-component droplets on solid surfaces, the effects of wall-mixture interactions on patterns in the bulk and the role of cross-coupling relaxation rates in controlling kinetic processes in both the bulk and surface.

According to the Gibbs rule, a ternary mixture system can have at most three coexisting phases in a system (see Appendix for details). In this section, we will evidence our points in both two-phase and three-phase coexisting scenarios.
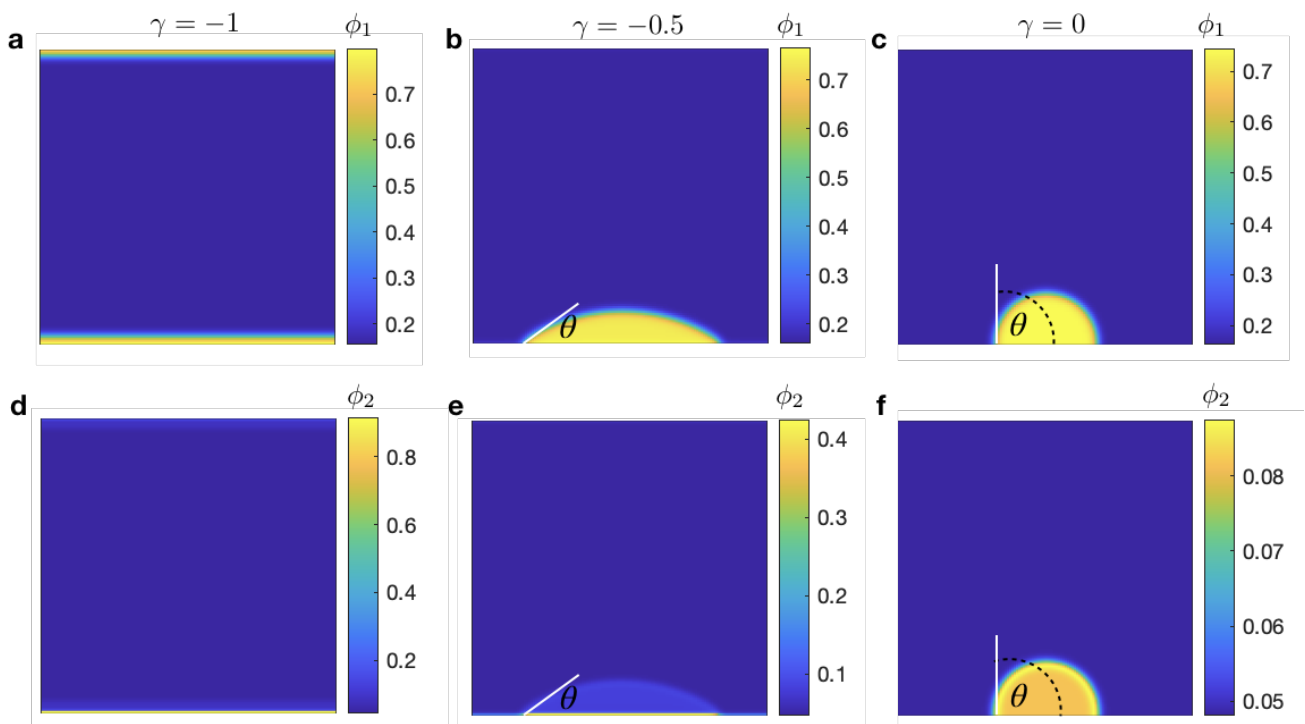
Figure 6. Profiles of ϕ_1 and ϕ_2 with a nonlinear coupling interaction between ϕ_1 and ϕ_2 in equilibrium. Plots (**a**, **b**, **c**) represent the concentration profiles of ϕ_1, while plots (**d**, **e**, **f**) represent the concentration profiles of ϕ_2. We observe that, as the negative coupling interaction between ϕ_1 and ϕ_2 becomes stronger, the contact angle decreases until the condensate (yellow) completely wets on the solid surface (plots (**a**, **d**). Here, we only investigate the negative coupling interaction since the positive coupling interaction will lead to nonphysical solutions. The basic parameter values used in this case are as follows: $\kappa_{1\Gamma} = \kappa_{2\Gamma} = 0$, $\kappa_1 = \kappa_2 = 1$, $h_1 = h_2 = g_1 = g_2 = 0$, $\chi_{12} = -1$, $\chi_{23} = 0$, $\chi_{13} = 2.5$.

4.1. Contact angle is determined by the additive effects of wall-mixture interaction

The contact angle is a measure of the wetting behavior of a liquid on a solid surface. It is determined by the balance of forces between the solid phase and two other liquid phases on the top of the solid surface. The wall-mixture interaction plays a significant role in determining the contact angle.
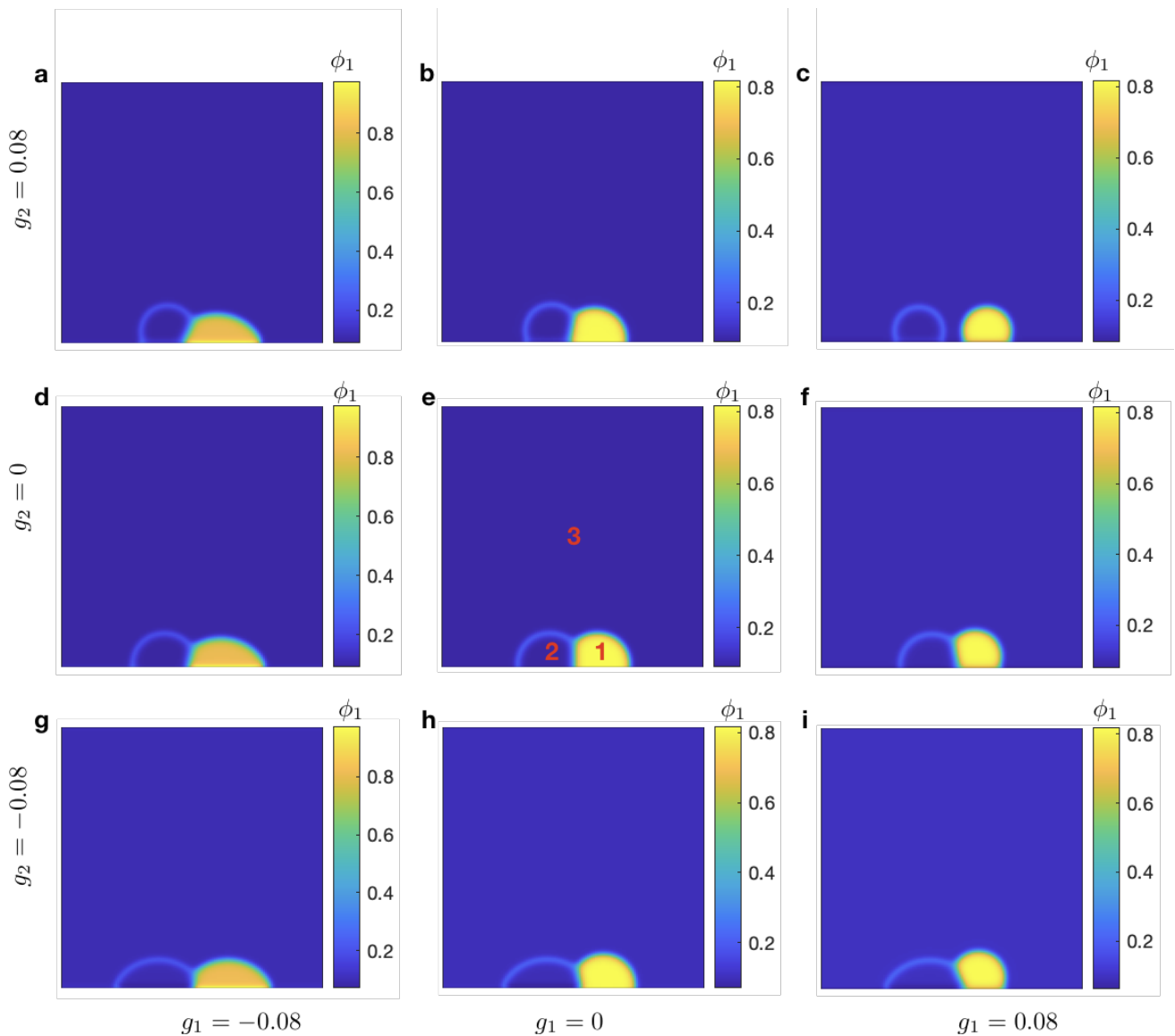
Figure 7. Profiles of ϕ_1 with a quadratic interaction between the solid wall and mixture components along the contact angle of a three-phase coexisting mixture at equilibrium. With the interaction parameter values $\chi_{12} = \chi_{23} = \chi_{13} = 3$, the ternary mixture has three coexisting phases (respectively denoted by red numbers 1, 2, 3 in plot **e**). We changed the strength of the quadratic interaction, i.e., the values of $g_i, i = 1, 2$. We observe that the contact angle of droplets 1 and 2 are mainly determined by the interaction between the dominant component and the solid wall, i.e., ϕ_1 in droplet 1 and ϕ_2 in droplet 2. Other basic parameter values used in this case are as follows: $\kappa_{1\Gamma} = \kappa_{2\Gamma} = 0$, $\kappa_1 = \kappa_2 = 1$, $h_1 = h_2 = \gamma = 0$.

In the case of a multi-component liquid mixture, the contact angle is determined by the combined effects of the interactions between the individual component of the mixture and the solid surface. To grasp these additive effects, we define the surface free energy as the summation of interactions between individual components and the solid wall.
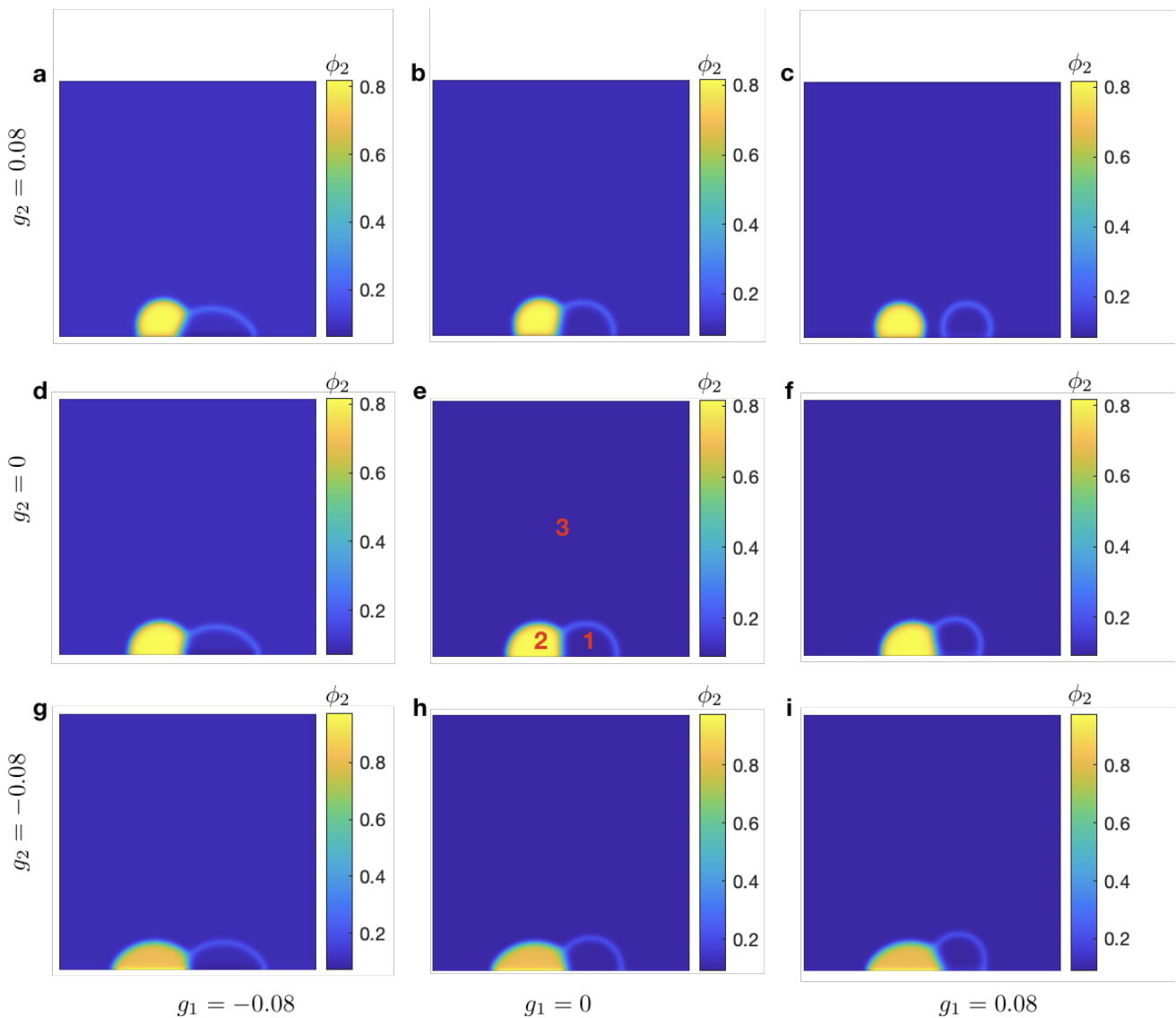
Figure 8. Profiles of ϕ_2 with a quadratic interaction between the solid wall and mixture components along the contact angle of a three-phase coexisting mixture at equilibrium. The basic parameter values used in this case are as follows: $\kappa_{1\Gamma} = \kappa_{2\Gamma} = 0$, $\kappa_1 = \kappa_2 = 1$, $h_1 = h_2 = \gamma = 0$, $\chi_{12} = \chi_{23} = \chi_{13} = 3$.

Specifically, the surface free energy is given by

$$f_s(\phi_{1\Gamma}, \phi_{2\Gamma}) = \frac{k_B T}{v_s}\Big[h_1\phi_{1\Gamma} + g_1\phi_{1\Gamma}^2 + h_2\phi_{2\Gamma} + g_2\phi_{2\Gamma}^2 + \gamma\phi_{1\Gamma}\phi_{2\Gamma}\Big]. \tag{4.1}$$

Here, $h_i\phi_i$ depicts the interaction between the solid wall and i-th component and $g_i\phi_i^2$ represents the interaction among i-th component molecules near the solid surface. $\gamma\phi_1\phi_2$ denotes the interaction between different kinds of molecules.

If all of the interactions mentioned above are mutual, i.e., $h_i = g_i = \gamma = 0$, the contact angle of droplets on the surface is 90º (see Figure 2e). If the interactions between each component and the solid wall are all attractive, i.e., $h_i < 0$, $g_i < 0$ or $\gamma < 0$, the contact angle will decrease until complete

wetting is achieved (see Figures 2–4, 5g and 6a,b), while repulsive interactions will lead to a larger contact angle, i.e., $\theta > 90^\circ$ (see Figures 2–4 and 5c). If interactions between individual components and the solid wall are different, e.g., the interaction between ϕ_1 and the solid wall is attractive, while the interaction between ϕ_2 and the solid wall is repulsive, the effective interaction between the droplet and solid wall is determined by the dominant component with a higher concentration in the droplet (see Figures 2–4 and 5a,i). These observations can be verified in the coexistence of the three phases (see Appendix) wetting phenomena (see Figures 7 and 8).
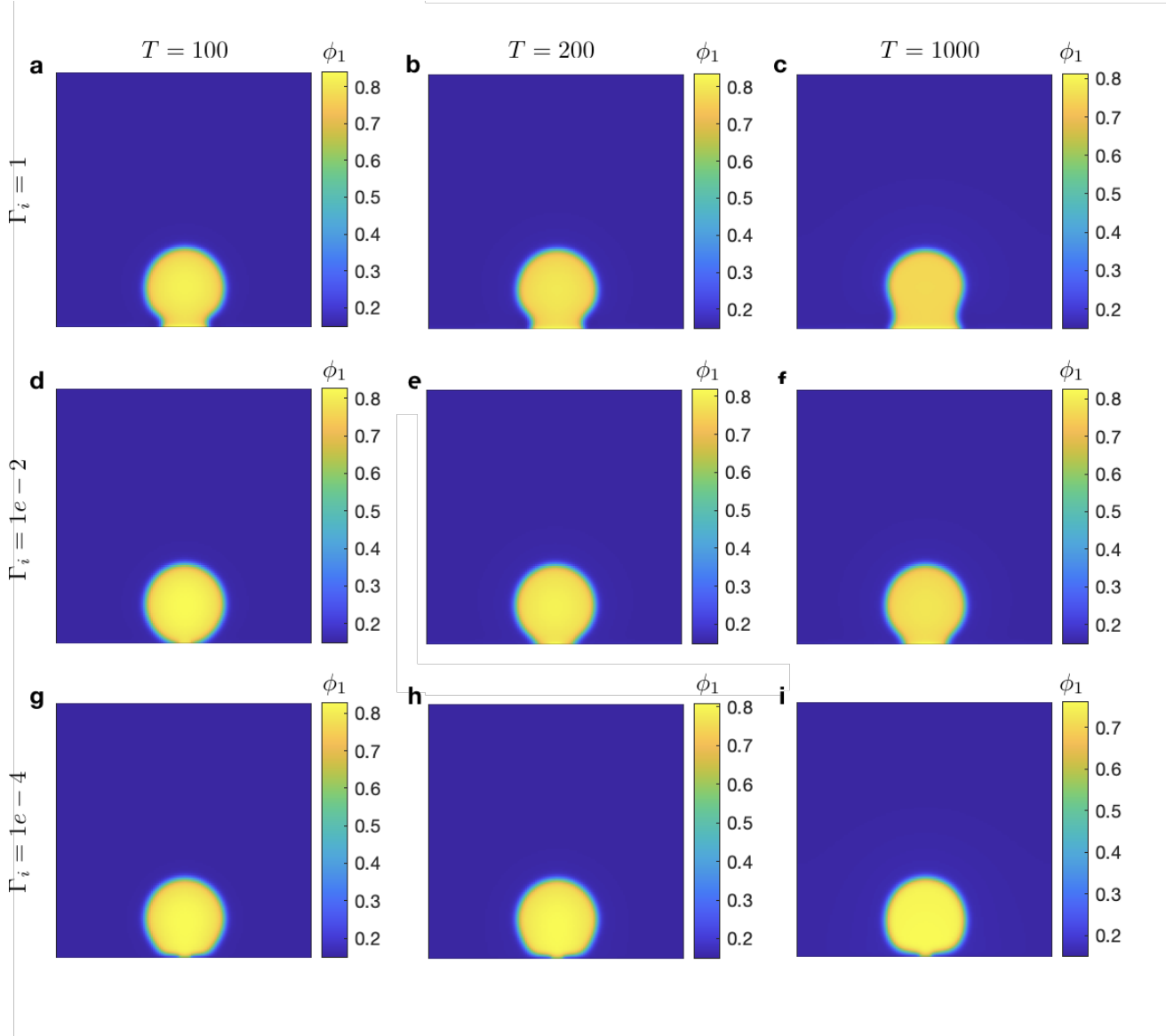
Figure 9. Relaxation of dynamic boundary conditions controls the droplet spreading on the surface. Plots (**a**–**i**) are the snapshots of component 1, i.e., ϕ_1. We do not consider the cross-coupling interaction in this simulation, i.e., $\Gamma_{12} = 0$. The relaxation rate Γ_i, $i = 1, 2$ decreases from 1 to 10^{-4}, and the spreading process slows down correspondingly. Other basic parameter values used in this case are as follows: $\kappa_{1\Gamma} = \kappa_{2\Gamma} = 0$, $\kappa_1 = \kappa_2 = 1$, $h_1 = 0$, $h_2 = 0$, $g_1 = -1$, $g_2 = 0$, $\gamma = 0$, $\chi_{12} = -1$, $\chi_{23} = 0$, $\chi_{13} = 2.5$.
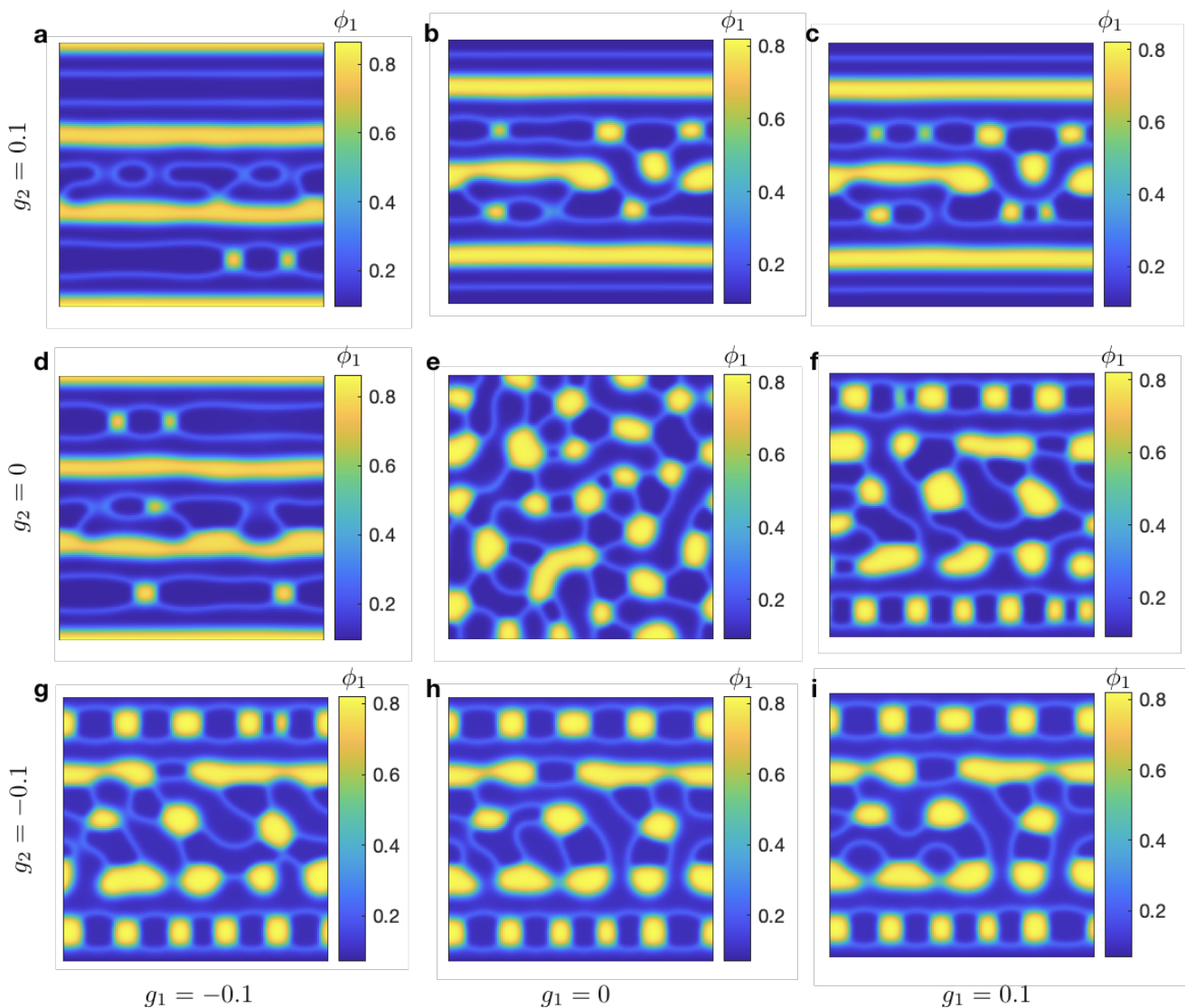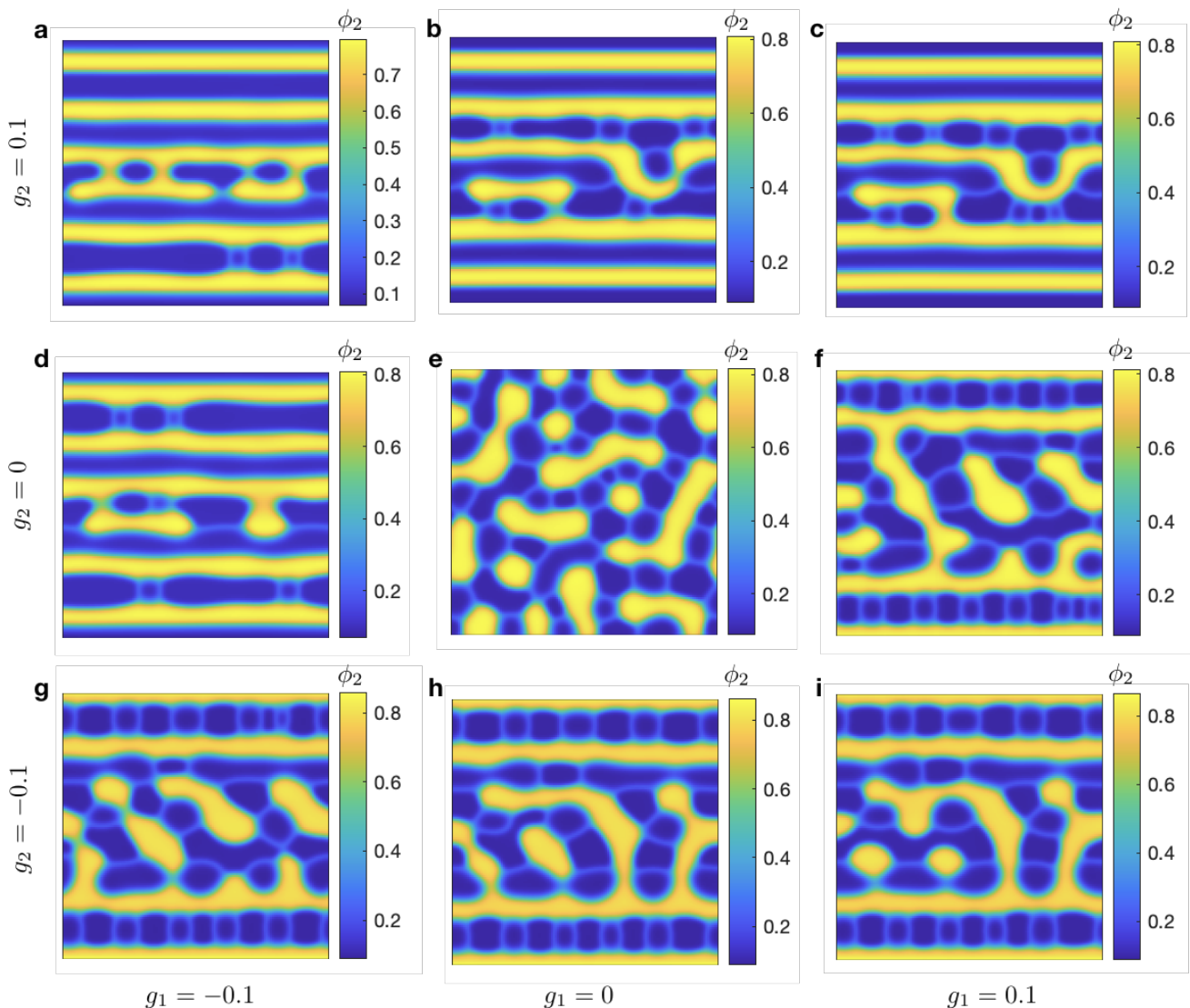
Figure 10. Profiles of ϕ_1 during the spontaneous phase separation of the ternary mixture with three-phase coexistence with various types of wall-mixture interactions. We show the snapshots of ϕ_1 at $T = 10,000$. Under the condition of neutral wall-mixture interaction (plot **e**, i.e., $g_i = 0, i = 1, 2$), the condensates (yellow) distribute in the bulk homogeneously. However, under the condition of attractive/repulsive wall-mixture interaction, the condensates distribute horizontally, parallel with the solid wall (see plots **a**, **b**, **c**, **d**, **f**, **g**, **i**). The basic parameter values used in this case are as follows: $h_1 = h_2 = 0$, $\kappa_{1\Gamma} = \kappa_{2\Gamma} = 1$, $\kappa_1 = \kappa_2 = 1$, $\gamma = 0$, $\chi_{12} = \chi_{23} = \chi_{13} = 3$.

4.2. Wall-mixture interaction changes the condensates patterns far away from the surface

The influence of wall-mixture interactions in the formation of condensate patterns in systems exhibiting three-phase coexistence has yet to be extensively investigated. This study aims to bridge this gap by delving into the phase separation and condensate coarsening processes within such systems, paying special attention to the varying types of wall-mixture interactions.

Our numerical studies revealed that interactions between the wall and the mixture exert a profound effect on the condensate patterns in the bulk, even in regions distant from the surface. We observed distinct variations in the condensate configurations that are contingent on the nature of the wall-mixture interactions. For instance, in cases in which strong attractive or repulsive forces were at play, the resultant patterns manifested as strips running parallel to the solid wall, as evidenced by Figures 10 and 11a–d. Conversely, when the interactions were weak, the patterns that emerged were less structured and more sporadic, as can be seen in Figures 10 and 11e. These findings underscore the significance of wall-mixture interactions in determining the arrangement of condensates within the bulk.
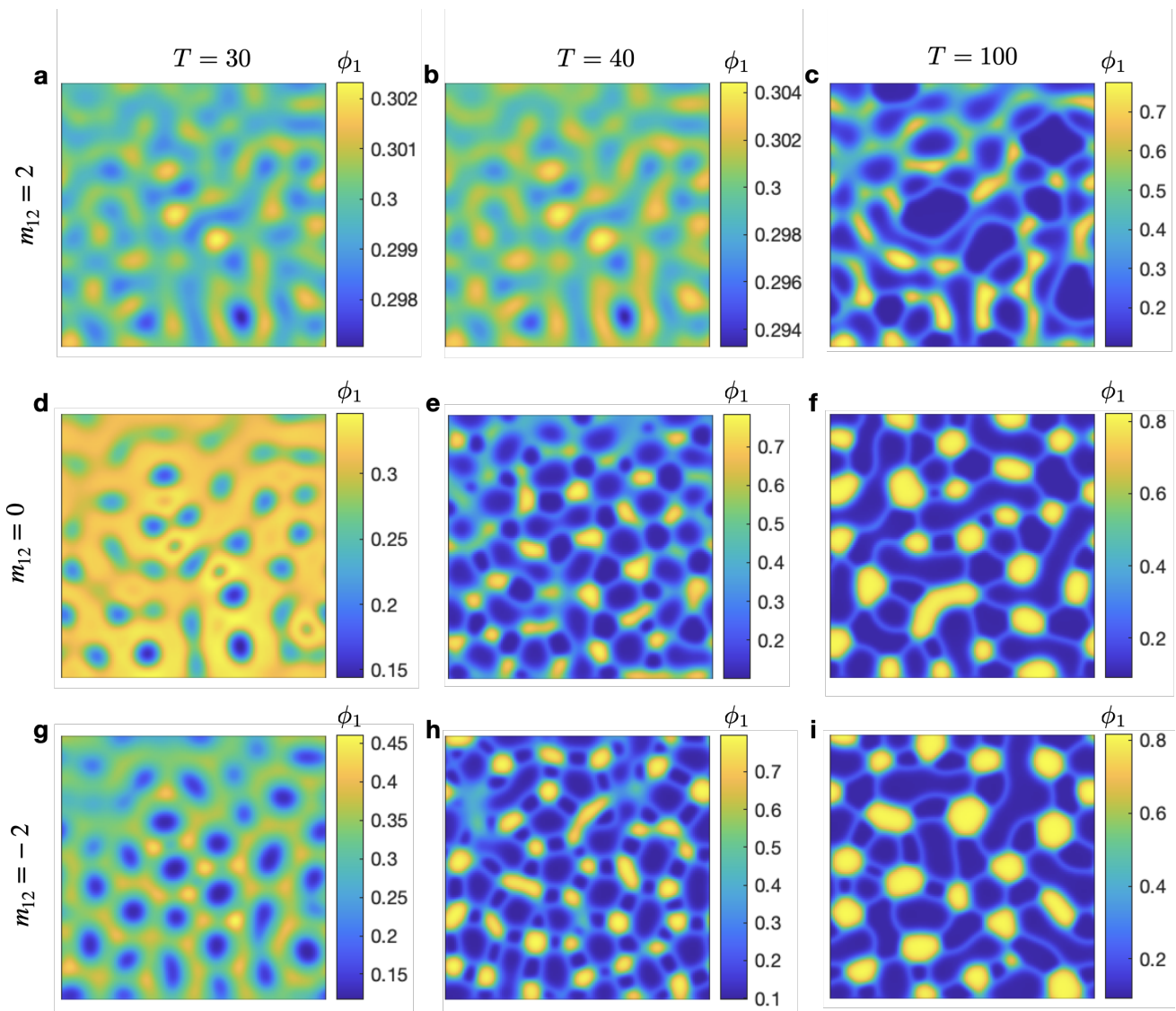

Figure 11. Profiles of ϕ_2 during the spontaneous phase separation of the ternary mixture with three-phase coexistence with various types of wall-mixture interactions. The basic parameter values used in this case are as follows: $h_1 = h_2 = 0$, $\kappa_{1\Gamma} = \kappa_{2\Gamma} = 1$, $\kappa_1 = \kappa_2 = 1$, $\gamma = 0$, $\chi_{12} = \chi_{23} = \chi_{13} = 3$.

## 4.3. Relaxation rate controls the kinetic process in the bulk and surface

The relaxation rate serves as a pivotal factor that influences the kinetic processes occurring within the bulk and on the surface of a system. To elucidate the impact of kinetic rates in the spreading of droplets on a solid surface, we placed a droplet atop the surface and varied the kinetic rates, denoted as Γ_i, from 10^{-4} to 1. Our observations revealed that the surface relaxation rates play a decisive role in dictating the kinetics of droplet spreading. Specifically, a faster surface relaxation rate accelerates the spreading of the droplet, as depicted in Figure 9.
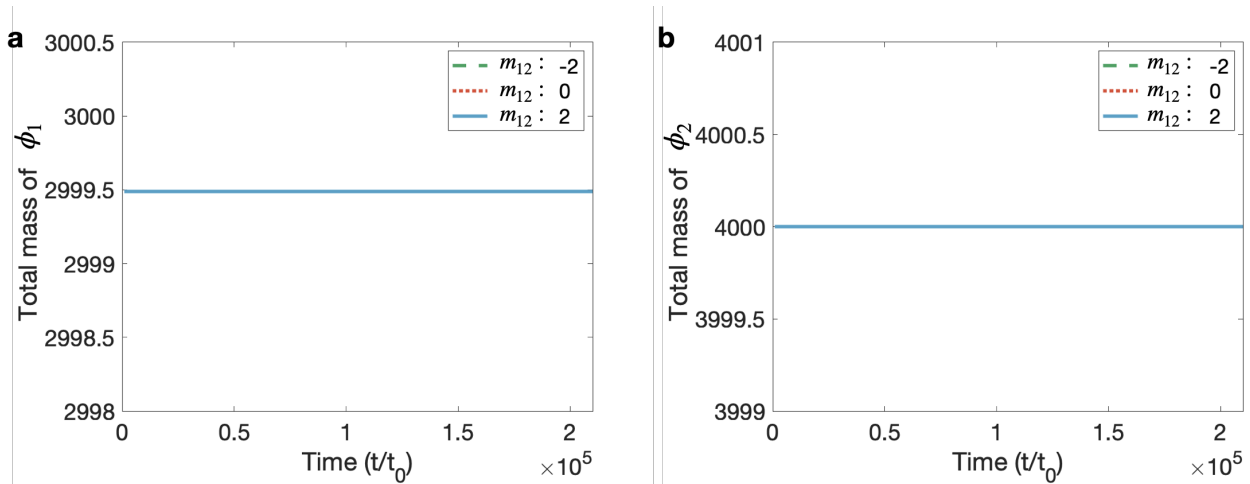

Figure 12. Profiles of ϕ_1 during spontaneous phase separation evolution at different time points with different values of the cross-coupling coefficient m_{12}. We find that changing the cross-coupling coefficient m_{12} leads to changes in the phase separation and following coarsening processes. The basic parameter values used in this study are as follows: $h_1 = h_1 = g_1 = g_2 = \gamma = 0$, $\kappa_{1\Gamma} = \kappa_{2\Gamma} = 1$, $\kappa_1 = \kappa_2 = 1$, $\gamma = 0$, $\chi_{12} = \chi_{23} = \chi_{13} = 3$.
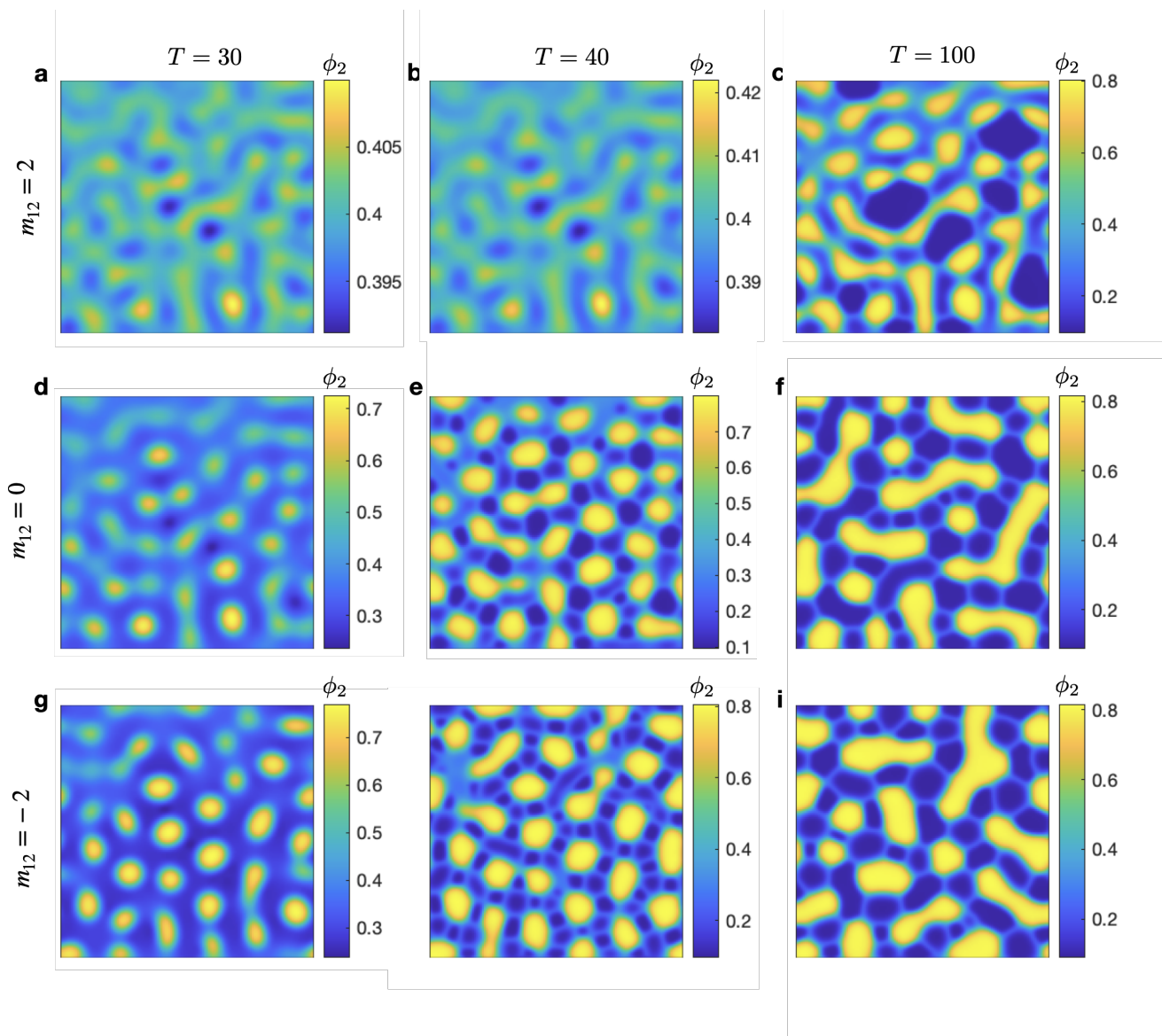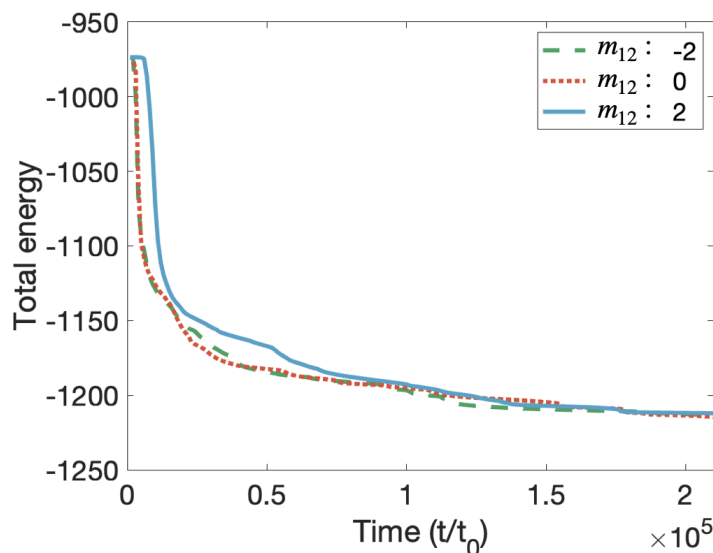
Figure 13. Profiles of ϕ_2 during spontaneous phase separation evolution at different time points with different values of cross-coupling coefficient m_{12}. The basic parameter values used in this case are as follows: $h_1 = h_1 = g_1 = g_2 = \gamma = 0$, $\kappa_{1\Gamma} = \kappa_{2\Gamma} = 1$, $\kappa_1 = \kappa_2 = 1$, $\gamma = 0, \chi_{12} = \chi_{23} = \chi_{13} = 3$.

The exploration of the effects of cross-coupling coefficients has been limited in previous research. In this study, we altered the cross-coupling coefficient, m_{12}, in the bulk to investigate its impact on the phase separation process therein. Our simulations indicate that changes in cross-coupling can indeed alter the kinetic processes (see Figures 12 and 13 for the snapshots). The total masses of ϕ_1 and ϕ_2 (see Figure 14) with different cross-coupling coefficient m_{12} values are constants, as proved by Theorem 3.3. From the total energy profiles (see Figure 15), it is evident that variations in m_{12} influence the total energy evolution during the initial stages of spontaneous phase separation. Further, we adjusted the cross-coupling coefficient on the surface, Γ_{12}, to scrutinize its effects on the kinetics of

droplet spreading on the solid surface. Our findings suggest that cross-coupling exerts a minimal effect on droplet spreading and coarsening subsequent to the phase separation process.

Figure 14. Total masses of ϕ_1 and ϕ_2 in the system during the spontaneous phase separation process. The basic parameter values used in this case are as follows: $h_1 = h_1 = g_1 = g_2 = \gamma = 0, \kappa_{1\Gamma} = \kappa_{2\Gamma} = 1, \kappa_1 = \kappa_2 = 1, \gamma = 0, \chi_{12} = \chi_{23} = \chi_{13} = 3$.

Figure 15. Total energy profiles during spontaneous phase separation process with different values of the cross-coupling coefficient m_{12}. The basic parameter values used in this case are as follows: $h_1 = h_1 = g_1 = g_2 = \gamma = 0, \kappa_{1\Gamma} = \kappa_{2\Gamma} = 1, \kappa_1 = \kappa_2 = 1, \gamma = 0, \chi_{12} = \chi_{23} = \chi_{13} = 3$.

5. Conclusions

In this paper, we have presented a systematic derivation of multi-component, multi-phase mixtures with dynamic boundary conditions. The governing equations in the models are composed of the mass conservation and constitutive equations, which are derived by using the Onsager principle to preserve the energy dissipation rate in time. The gradient flow structure is $H^{-1}(\Omega)$ in the bulk and $L_2(\Gamma)$ on the surface.

Moreover, we have presented a second-order, fully discrete, linear and unconditionally energy-stable numerical scheme for the ternary mixture model with dynamic boundary conditions. First, we reformulate the model by introducing intermediate variables by implementing the IEQ strategy. Using the reformulated model equations, we develop a second-order, energy-stable, semi-discrete numerical scheme in time. Then, we obtain a fully discrete numerical scheme by applying the finite-difference method to the staggered grid in space, which preserves a fully discrete energy dissipation rate and the total mass conservation laws.

Beyond theoretical advancements, our work has substantial engineering implications. Utilizing our efficient and accurate numerical solver, we have investigated the effects of short-ranged interaction between the mixture components and solid surface on the wettability of the surface, from the perspectives of both stationary and kinetic solutions. We found that the contact angle of condensates are determined by the additive effects introduced by the interaction between each component and the solid wall. The droplet spreading can be affected hugely by the surface relaxation rates, while the cross-coupling relaxation rate for the surface does not influence the droplet spreading a lot. Furthermore, the spontaneous phase separation phenomena of ternary mixtures with two phases and three phases, and subject to dynamic boundary conditions, have been explored. Our results suggest that strong attractive/repulsive coupling between the surface and bulk leads to ordered condensate patterns in the bulk. Moreover, the cross-coupling in the bulk changes the phase separation process significantly. This insight is invaluable in fields like semiconductor manufacturing, where surface properties are critical, or in medical device fabrication, where understanding biofluid interactions with surfaces can lead to better product designs.

Furthermore, our model and the scheme can be readily extended to models of N-component mixtures with $N > 3$. Our work provides a general framework for the study of multi-component mixtures with dynamic boundary conditions. The multi-component mixtures with more complex boundary conditions, e.g., those developed as Goldstein (1.6), Liu-Wu model (1.7) and KLLM model (1.8), can be studied based on this framework. This work not only provides a foundational framework for future study of multi-component mixtures with dynamic boundary conditions for a wide range of applications, it also exerts a significant influence in the study of complex fluid dynamics.

Use of AI tools declaration

The authors declare that they have not used artificial intelligence tools in the creation of this article.

Acknowledgments

thank the anonymous referees for their critical comments.

Conflict of interest

The authors declare that there is no conflict of interest.

References

1. C. Brangwynne, C. R. Eckmann, D. S. Courson, A. Rybarska, C. Hoege, J. Gharakhani, et al., Germline p granules are liquid droplets that localize by controlled dissolution/condensation, *Science*, **324** (2009), 1729–1732. https://doi.org/10.1126/science.1172046

2. J. G. Gall, M. Bellini, Z. Wu, C. Murphy, Assembly of the nuclear transcription and processing machinery: cajal bodies (coiled bodies) and transcriptosomes, *Mol. Biol. Cell*, **10** (1999), 4385–4402. https://doi.org/10.1091/mbc.10.12.4385

3. J. Agudo-Canalejo, S. W. Schultz, H. Chino, S. M. Migliano, C. Saito, I. Koyama-Honda, et al., Wetting regulates autophagy of phase-separated compartments and the cytosol, *Nature*, **591** (2021), 142–146. https://doi.org/10.1038/s41586-020-2992-3

4. P. Tabeling, *Introduction to Microfluidics*, Oxford University Press, 2005.

5. F. Bruder, R. Brenn, Spinodal decomposition in thin films of a polymer blend, *Phys. Rev. Lett.*, **69** (1992), 624–627. https://doi.org/10.1103/PhysRevLett.69.624

6. G. Krausch, C. Dai, E. J. Kramer, F. S. Bates, Real space observation of dynamic scaling in a critical polymer mixture, *Phys. Rev. Lett.*, **71** (1993), 3669–3672. https://doi.org/10.1103/PhysRevLett.71.3669

7. L. Sung, A. Karim, J. F. Douglas, C. C. Han, Dimensional crossover in the phase separation kinetics of thin polymer blend films, *Phys. Rev. Lett.*, **76** (1996), 4368–4371. https://doi.org/10.1103/PhysRevLett.76.4368

8. A. K. Gunstensen, D. H. Rothman, S. Zaleski, G. Zanetti, Lattice Boltzmann model of immiscible fluids, *Phys. Rev. A*, **43** (1991), 4320–4327. https://doi.org/10.1103/PhysRevA.43.4320

9. X. Shan, H. Chen, Lattice Boltzmann model for simulating flows with multiple phases and components, *Phys. Rev. E*, **47** (1993), 1815–1819. https://doi.org/10.1103/PhysRevE.47.1815

10. X. Shan, H. Chen, Simulation of nonideal gases and liquid-gas phase transitions by the lattice Boltzmann equation, *Phys. Rev. E*, **49** (1994), 2941–2948. https://doi.org/10.1103/PhysRevE.49.2941

11. M. R. Swift, W. R. Osborn, J. M. Yeomans, Lattice Boltzmann simulation of nonideal fluids, *Phys. Rev. Lett.*, **75** (1995), 830–833. https://doi.org/10.1103/PhysRevLett.75.830

12. M. R. Swift, E. Orlandini, W. R. Osborn, J. M. Yeomans, Lattice Boltzmann simulations of liquid-gas and binary fluid systems, *Phys. Rev. E*, **54** (1996), 5041–5052. https://doi.org/10.1103/PhysRevE.54.5041

13. S. Schmieschek, J. Harting, Contact angle determination in multicomponent lattice boltzmann simulations, *Commun. Comput. Phys.*, **9** (2011), 1165–1178. https://doi.org/10.4208/cicp.201009.271010s

14. G. Yan, Z. Li, T. Bore, S. A. G. Torres, A. Scheuermann, L. Li, Discovery of dynamic two-phase flow in porous media using two-dimensional multiphase lattice Boltzmann simulation, *Energies*, **14** (2021), 4044. https://doi.org/10.3390/en14134044

15. G. Yan, Z. Li, T. Bore, S. A. G. Torres, A. Scheuermann, L. Li, A lattice Boltzmann exploration of two-phase displacement in 2D porous media under various pressure boundary conditions, *J. Rock Mech. Geotech. Eng.*, **14** (2022), 1782–1798. https://doi.org/10.1016/j.jrmge.2022.05.003

16. H. Liang, J. Xu, J. Chen, Z. Chai, B. Shi, Lattice Boltzmann modeling of wall-bounded ternary fluid flows, *Appl. Math. Modell.*, **73** (2019), 487–513. https://doi.org/10.1016/j.apm.2019.03.009

17. A. Ferrari, I, Lunati, Direct numerical simulations of interface dynamics to link capillary pressure and total surface energy, *Adv. Water Resour.*, **57** (2013), 19–31. https://doi.org/10.1016/j.advwatres.2013.03.005

18. A. Ferrari, I, Lunati, Inertial effects during irreversible meniscus reconfiguration in angular pores, *Adv. Water Resour.*, **74** (2014), 1–13. https://doi.org/10.1016/j.advwatres.2014.07.009

19. A. Ferrari, J. Jimenez-Martinez, T. L. Borgne, Y. Méheust, I. Lunati, Challenges in modeling unstable two-phase flow experiments in porous micromodels, *Water Resour. Res.*, **51** (2015), 1381–1400. https://doi.org/10.1002/2014WR016384

20. Z. Li, S. Galindo-Torres, A. Scheuermann, L. Li, Mesoscopic approach to fluid-solid interaction: Apparent liquid slippage and its effect on permeability estimation, *Phys. Rev. E*, **98** (2018), 052803. https://doi.org/10.1103/PhysRevE.98.052803

21. Z. Li, J. Li, G. Yan, S. Galindo-Torres, A. Scheuermann, L. Li, Mesoscopic model framework for liquid slip in a confined parallel-plate flow channel, *Phys. Rev. Fluids*, **6** (2021), 034203. https://doi.org/10.1103/PhysRevFluids.6.034203

22. J. W. Cahn, J. E. Hilliard, Free energy of a nonuniform system. I. interfacial free energy, *J. Chem. Phys.*, **28** (1958), 258–267. https://doi.org/10.1063/1.1744102

23. J. W. Cahn, On spinodal decomposition in cubic crystals, *Acta Metall.*, **10** (1962), 179–183. https://doi.org/10.1016/0001-6160(62)90114-1

24. F. Eliot, E. G. Morton, Continuum theory of thermally induced phase transitions based on an order parameter, *Physica D*, **68** (1993), 326–343. https://doi.org/10.1016/0167-2789(93)90128-N

25. F. Bai, C. M. Elliott, A. Gardiner, A. Spence, A. M. Stuart, The viscous Cahn–Hilliard equation. I. Computations, *Nonlinearity*, **8** (1995), 131–160. https://doi.org/10.1088/0951-7715/8/2/002

26. M. E. Gurtin, Generalized Ginzburg-Landau and Cahn-Hilliard equations based on a microforce balance, *Physica D*, **92** (1996), 178–192. https://doi.org/10.1016/0167-2789(95)00173-5

27. H. P. Fischer, P. Maass, W. Dieterich, Novel surface modes in spinodal decomposition, *Phys. Rev. Lett.*, **79** (1997), 893–896. https://doi.org/10.1103/PhysRevLett.79.893

28. R. Kenzler, F. Eurich, P. Maass, B. Rinn, J. Schropp, E. Bohl, et al., Phase separation in confined geometries: Solving the Cahn–Hilliard equation with generic boundary conditions, *Comput. Phys. Commun.*, **133** (2001), 139–157. https://doi.org/10.1016/S0010-4655(00)00159-4

29. R. G. Gisèle, M. Alain, S. Giulio, A Cahn–Hilliard model in a domain with non-permeable walls, *Physica D*, **240** (2011), 754–766. https://doi.org/10.1016/j.physd.2010.12.007

30. C. Liu, H. Wu, A Cahn–Hilliard model in a domain with non-permeable walls, *Arch. Ration. Mech. Anal.*, **233** (2019), 167–247. https://doi.org/10.1007/s00205-019-01356-x

31. P. Knopf, K. F. Lam, C. Liu, S. Metzger, Phase-field dynamics with transfer of materials: The Cahn–Hilliard equation with reaction rate dependent dynamic boundary conditions, *ESAIM Math. Model. Numer. Anal.*, **55** (2021), 229–282. https://doi.org/10.1051/m2an/2020090

32. K. Binder, H. L. Frisch, Dynamics of surface enrichment: A theory based on the Kawasaki spin-exchange model in the presence of a wall, *Z. Phys. B: Condens. Matter*, **84** (1991), 403–418. https://doi.org/10.1007/BF01314015

33. S. Puri, K. Binder, Surface effects on spinodal decomposition in binary mixtures and the interplay with wetting phenomena, *Phys. Rev. E*, **49** (1994), 5359–5377. https://doi.org/10.1103/PhysRevE.49.5359

34. H. Garcke, P. Knopf, S. Yayla, Long-time dynamics of the Cahn–Hilliard equation with kinetic rate dependent dynamic boundary conditions, *Nonlinear Anal.*, **215** (2022), 112619. https://doi.org/10.1016/j.na.2021.112619

35. H. Wu, A review on the Cahn–Hilliard equation: classical results and recent advances in dynamic boundary conditions, *Electron. Res. Arch.*, **30** (2022), 2788–2832. https://doi.org/10.3934/era.2022143

36. T. Fukao, S. Yoshikawa, S. Wada, Structure-preserving finite difference schemes for the Cahn-Hilliard equation with dynamic boundary conditions in the one-dimensional case, *Commun. Pure Appl. Anal.*, **16** (2017), 1915–1938. https://doi.org/10.3934/cpaa.2017093

37. X. Meng, X. Bao, Z. Zhang, Second order stabilized semi-implicit scheme for the Cahn–Hilliard model with dynamic boundary conditions, *J. Comput. Appl. Math.*, **428** (2023), 115145. https://doi.org/10.1016/j.cam.2023.115145

38. J. M. Park, R. Mauri, P. D. Anderson, Phase separation of viscous ternary liquid mixtures, *Chem. Eng. Sci.*, **80** (2023), 270–278. https://doi.org/10.1016/j.ces.2012.06.017

39. A. Lamorgese, R. Mauri, Diffusion-driven dissolution or growth of a liquid drop embedded in a continuous phase of another liquid via phase-field ternary mixture model, *Langmuir*, **33** (2017), 13125–13132. https://doi.org/10.1021/acs.langmuir.7b02105

40. A. Lamorgese, R. Mauri, Dissolution or growth of a liquid drop via phase-field ternary mixture model based on the non-random, two-liquid equation, *Langmuir*, **20** (2018), 125. https://doi.org/10.3390/e20020125

41. Y. Li, J. Choi, J. Kim, Multi-component Cahn–Hilliard system with different boundary conditions in complex domains, *J. Comput. Phys.*, **323** (2016), 1–16. https://doi.org/10.1016/j.jcp.2016.07.017

42. J. Yang, Y. Li, J. Kim, Modified multi-phase diffuse-interface model for compound droplets in contact with solid, *J. Comput. Phys.*, **491** (2023), 112345. https://doi.org/10.1016/j.jcp.2023.112345

43. C. Zhang, H. Ding, P. Gao, Y. Wu, Diffuse interface simulation of ternary fluids in contact with solid, *J. Comput. Phys.*, **309** (2016), 37–51. https://doi.org/10.1016/j.jcp.2015.12.054

44. L. Onsager, Reciprocal relations in irreversible processes. I., *Phys. Rev.*, **37** (1931), 405–426. https://doi.org/10.1103/PhysRev.37.405

45. L. Onsager, Reciprocal relations in irreversible processes. II., *Phys. Rev.*, **38** (1931), 2265–2279. https://doi.org/10.1103/PhysRev.38.2265

46. X. Yang, J. Li, G. Forest, Q. Wang, Hydrodynamic theories for flows of active liquid crystals and the generalized Onsager principle, *Entropy*, **18** (2016), 202. https://doi.org/10.1103/PhysRev.38.2265

47. P. Sheng, J. Zhang, C. Liu, Onsager principle and electrorheological fluid dynamics, *Prog. Theor. Phys. Suppl.*, **175** (2008), 131–143. https://doi.org/10.1143/PTPS.175.131

48. M. Doi, Onsager principle in polymer dynamics, *Prog. Polym. Sci.*, **112** (2021), 101339. https://doi.org/10.1016/j.progpolymsci.2020.101339

49. F. Jülicher, J. Prost, Generic theory of colloidal transport, *Eur. Phys. J. E*, **29** (2009), 27–36. https://doi.org/10.1140/epje/i2008-10446-8

50. X. Yang, J. Zhao, Q. Wang, J. Shen, Numerical approximations for a three-component Cahn–Hilliard phase-field model based on the invariant energy quadratization method, *Math. Models Methods Appl. Sci.*, **27** (2017), 1993–2030. https://doi.org/10.1142/S0218202517500373

51. X. Yang, D. Han, Linearly first- and second-order, unconditionally energy stable schemes for the phase field crystal equation, *J. Comput. Phys.*, **333** (2017), 1116–1134. https://doi.org/10.1016/j.jcp.2016.10.020

52. J. Zhao, X. Yang, J. Li, Q. Wang, Energy stable numerical schemes for a hydrodynamic model of Nematic liquid crystals, *SIAM J. Sci. Comput.*, **38** (2016), A3264–A3290. https://doi.org/10.1137/15M1024093

53. J. Zhao, X. Yang, Y. Gong, X. Zhao, X. Yang, J. Li, et al., A general strategy for numerical approximations of non-equilibrium models–Part I: Thermodynamical systems, *Int. J. Numer. Anal. Mod.*, **15** (2018), 884–918.

54. J. W. Cahn, Critical point wetting, *J. Chem. Phys.*, **66** (1977), 3667–3672. https://doi.org/10.1063/1.434402

55. X. Zhao, Q. Wang, A second order fully-discrete linear energy stable scheme for a binary compressible viscous fluid model, *J. Comput. Phys.*, **395** (2019), 382–409. https://doi.org/10.1016/j.jcp.2019.06.030

Appendix

Phase diagram of ternary mixture

We chose to use a convex hull algorithm to calculate the phase diagram of the ternary mixture. The interaction parameters values are $\chi_{12} = \chi_{23} = \chi_{13} = 3$, and the wall-mixture interaction coefficients and $h_1 = h_2 = g_1 = g_2 = \gamma = 0$.
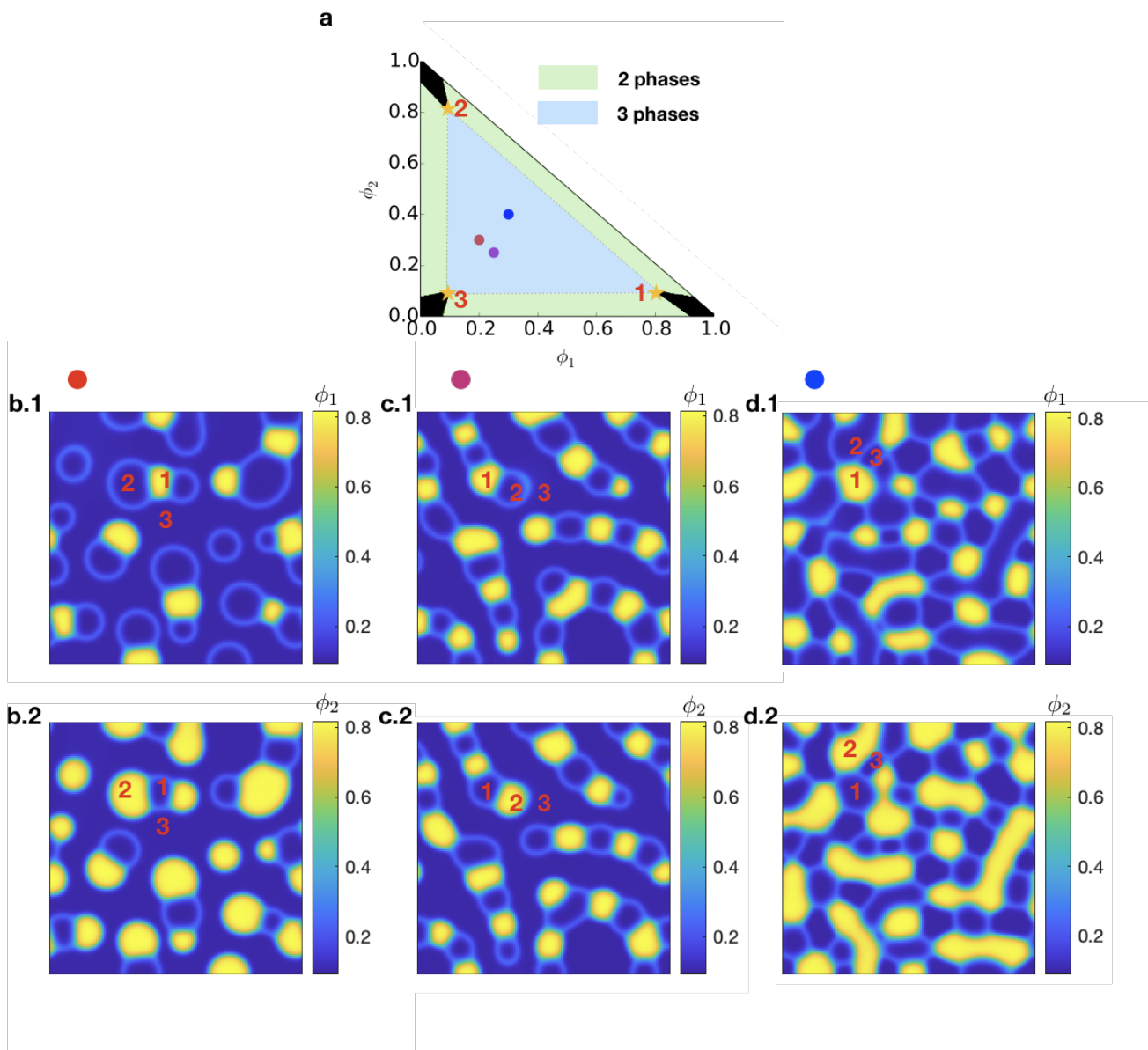
Figure A1. Phase diagrams of the ternary mixture and three-phase coexistence examples. Plot **a** is the phase diagram of the ternary mixture. Black region depicts the case with one homogeneous phase; green region depicts the case with two phases; blue region denotes the case with three coexisting phases. Plots **b.1**–**b.2**, **c.1**–**c.2**, **d.1**–**d.2** are snapshots of ϕ_1 and ϕ_2 with different sets of the initial composition, which are marked by the color dots in the blue region. The basic parameter values used in this case are as follows: $h_1 = 0, h_2 = 0$, $\kappa_1 = \kappa_2 = 1, g_1 = g_2 = \gamma = 0, \chi_{12} = \chi_{23} = \chi_{13} = 3$.

In the phase diagram Figure A1, the x axis represents the composition of one of the components ϕ_1 in the mixture, while the y axis represents the composition of another component ϕ_2. The concentration of the third component equals $1 - \phi_1 - \phi_2$ based on the incomprehensibility assumption. This phase diagram depicts the behavior of the ternary mixture at equilibrium. The black regions represent the mixture, which has no phase separation at equilibrium. The ternary mixture, which has the compo-

sitions shown in the light green regions, will phase-separate into two coexisting phases with different composition profiles. In the blue region, there are three coexisting phases. The compositions of these three phases are denoted by the yellow stars in the three corners of the region. Here, we give three examples of three-phase coexisting ternary mixtures, which are depicted by three colorful dots (red, magenta, blue). Correspondingly, in Figure A1b.1–d.2, we show the three-phase coexisting system with phases 1, 2, 3. Specifically, Figure A1b.1,c.1,d.1 show the concentration profiles of ϕ_1 in each case, while Figure A1b.2,c.2,d.2 the concentration profiles of ϕ_2. All of the numerical simulations of three-phase coexisting phenomena in the main text are based on this phase diagram.